

## THE GLOBAL STAR FORMATION LAWS OF GALAXIES FROM A RADIO CONTINUUM PERSPECTIVE

L. LIU<sup>1,2,4</sup>, Y. GAO<sup>1</sup>, T.R. GREVE<sup>3</sup>,

*Draft version August 8, 2021*

### ABSTRACT

We study the global star formation law - the relation between gas and star formation (SF) rates in a sample of 181 local galaxies with infrared (IR) luminosities spanning almost five orders of magnitude ( $10^{7.8} - 10^{12.3} L_{\odot}$ ), which includes 115 normal spiral galaxies and 66 (ultra)luminous IR galaxies [(U)LIRGs,  $L_{\text{IR}} \geq 10^{11} L_{\odot}$ ]. We derive their atomic, molecular gas and dense molecular gas masses using newly available HI, CO and HCN data from the literature, and SF rates are determined both from total IR (8 – 1000  $\mu\text{m}$ ) and 1.4 GHz radio continuum (RC) luminosities. In order to derive the disk-averaged surface densities of gas and SF rates, we have taken a novel approach and used high-resolution RC observations to measure the radio sizes for all 181 galaxies. In our sample, we find that the surface density of dense molecular gas (as traced by HCN) has the tightest correlation with that of SF rates ( $\Sigma_{\text{SFR}}$ ), and is linear in log – log space (power-law slope of  $N = 1.01 \pm 0.02$ ) across the full galaxy sample. The correlation between surface densities of molecular gas ( $\Sigma_{\text{H}_2}$ , traced by CO) and  $\Sigma_{\text{SFR}}$  is sensitive to the adopted value of the CO-to-H<sub>2</sub> conversion factor ( $\alpha_{\text{CO}}$ ) used to infer molecular gas masses from CO luminosities. For a fixed Galactic value of  $\alpha_{\text{CO}}$ , a power law index of  $1.14 \pm 0.02$  is found. If instead we adopt values for  $\alpha_{\text{CO}}$  of 4.6 and 0.8 for disk galaxies and (U)LIRGs, respectively, we find the two galaxy populations separate into two distinct  $\Sigma_{\text{SFR}}$  versus  $\Sigma_{\text{H}_2}$  relations. Finally, applying a continuously varying  $\alpha_{\text{CO}}$  to our sample, we recover a single  $\Sigma_{\text{SFR}}$ - $\Sigma_{\text{H}_2}$  relation with slope of  $1.60 \pm 0.03$ . The  $\Sigma_{\text{SFR}}$  is a steeper function of total gas  $\Sigma_{\text{gas}}$  (molecular gas with atomic gas) than that of molecular gas  $\Sigma_{\text{H}_2}$ , and are tighter among low-luminosity galaxies. We find no correlation between global surface densities of SFRs and atomic gas (HI).

*Subject headings:* galaxies: low-redshift, high-redshift — galaxies: formation — galaxies: evolution — galaxies: starbursts — radio

### 1. INTRODUCTION

The notion of a general so-called star formation (SF) law applicable to galaxies was first introduced by Schmidt (1959), who suggested that the star formation rate (SFR) volume density ( $\rho_{\text{SFR}}$ ) varies with the interstellar gas volume density ( $\rho_{\text{gas}}$ ) as a power law, i.e.  $\rho_{\text{SFR}} \propto \rho_{\text{gas}}^N$ , where  $N \sim 2$ . Under the assumption of a constant scale-height for the star forming gas, this relation translates directly into an equivalent expression for the SFR and gas surface density,  $\Sigma_{\text{SFR}} \propto \Sigma_{\text{gas}}^N$ , which can be determined from observations. In a seminal study of the SFR (traced by H $\alpha$ ) and gas (traced by HI and CO) distributions in a sample of nearby galaxies, Kennicutt (1998) (K98 hereafter) found  $N \sim 1.4 \pm 0.2$ . Nevertheless, discrepancies widely exist in the power-law index (e.g., Bouché et al. 2007; Bigiel et al. 2008; Blanc et al. 2009; Verley et al. 2010). The exact functional form of the SF law has important implications for our understanding of the physical processes that govern SF in galaxies (Krumholz et al. 2012) and also plays an important role in the evolution of global galaxy properties

(Feldmann 2013)

In recent years, the increases in receiver sensitivities have allowed for high-resolution maps of the SFR and gas distribution, and thus made probing the spatially resolved SF law on sub-kpc scales in nearby galaxies achievable. (e.g., Wong & Blitz 2002; Kennicutt et al. 2007; Bigiel et al. 2008, 2011; Blanc et al. 2009; Schrubba et al. 2010, 2011; Rahman et al. 2012). Such detailed studies provide important insights into the physical processes governing the SF. However, they are rarely feasible in the distant Universe, and have only been achieved in a few local (ultra)luminous IR galaxies [(U)LIRGs,  $L_{\text{IR}} \geq 10^{11} L_{\odot}$ ] (e.g., Boquien et al. 2011) and high- $z$  galaxies (e.g., Hodge et al. 2012). Instead, the global galaxy-averaged measurements, covering a large range of galaxies with extremely distributed SFRs and gas densities, provide a powerful way of characterising the SF law as a function of galaxy-wide properties.

A critical aspect of determining the global SF law is the ability to accurately measure the physical size of the star forming region within galaxies. Past studies have used a variety of optical, IR and CO imaging to determine the extent of star forming areas. In K98, where a total of more than 90 local galaxies were studied (most are normal spiral galaxies, with  $\sim 10$  (U)LIRGs), the sizes used to normalize the total SFRs and gas masses for the subset of normal galaxies were determined from optical images, while the sizes of IR starbursts were determined from CO or IR maps. Determining the physical sizes of star forming regions in high- $z$  galaxies turned out

ljliu@mpifri-bonn.mpg.de, yugao@pmo.ac.cn

<sup>1</sup> Purple Mountain Observatory, Key Lab of Radio Astronomy, 2 West Beijing Road, 210008 Nanjing, PR China

<sup>2</sup> Max-Planck-Institut für Radioastronomie, Auf dem Hügel 69, D-53121 Bonn, Germany

<sup>3</sup> Department of Physics and Astronomy, University College London, Gower Street, London WC1E 6BT, UK

<sup>4</sup> University of Chinese Academy of Sciences, 19A Yuquan Road, PO Box 3908, 100039 Beijing, PR China

to be a much bigger challenge due to its requirement for higher resolution and sensitivity. As a result, the high- $z$  studies, as well as local studies, usually adopted different methods in different wavebands in deducing the sizes for the various sub-samples. This would inevitably introduce systematic uncertainties. Thus, it is necessary to introduce a uniform way to determine the physical scales of both local and high- $z$  galaxies.

In the work presented here, we revisit the local SF law based on a dataset nearly twice as large as that of K98, and we use high-resolution radio continuum (RC) maps exclusively to infer the sizes of star forming areas and their SFRs. The radio is an excellent tracer of SF. It is extinction-free and exhibits an extraordinarily tight correlation with far-IR light ( $\sim 0.3$  dex scatter over five orders of magnitude in luminosity) (Condon et al. 1991; Yun et al. 2001; Murphy et al. 2006b), which shows little or no evolution over the redshift range  $z = 0 - 2$  (Sargent et al. 2010; Bourne et al. 2011; Mao et al. 2011). Spatially resolved measurements of local star forming galaxies in the radio and far-IR have shown that this tight relationship extends down to  $\lesssim 1$  kpc within disks (Murphy et al. 2006a,b, 2008). Similar observations of early-type galaxies show a striking agreement between the radio, mid-IR ( $24\mu\text{m}$ ) and CO morphologies (Lucero & Young 2007; Young et al. 2009). The highest resolution of radio interferometers (e.g., (J)VLA, eMerlin) can resolve even the most compact nearby starburst galaxies (Condon et al. 1996; Carilli et al. 1998; Carilli & Taylor 2000; Pihlström et al. 2001; Momjian et al. 2003). We therefore expect our radio-inferred galaxy sizes to accurately match the star forming regions in various types of galaxies in our sample.

Millimeter and IR observations of giant molecular clouds (GMCs) in our Galaxy have shown that stars form in dense cores, and that massive stars form almost exclusively in clumps/clusters of massive dense cores (Evans 1999, 2008; Wu et al. 2010). The dense gas ( $n > 10^4 \text{ cm}^{-3}$ ) residing in these cores is best traced by molecules with high-dipole moments and thus high critical densities, such as HCN and CS. Gao & Solomon (2004a,b) (GS04a,b hereafter) carried out the first systematic HCN survey of a large local galaxy sample and found a tight linear correlation between the IR and HCN luminosities spanning three orders of magnitude. More recent studies, targeting not just HCN but also other high-density gas tracers (e.g.  $\text{HCO}^+$ , HNC, CN and CS) in local galaxies, also find molecular line luminosities linearly increasing with IR luminosity ( $L_{\text{IR}}$ ) (Baan et al. 2008; Krips et al. 2008; Juneau et al. 2009; Matsushita et al. 2010; Zhang et al. 2014). Here, we also present an analysis of the dense gas SF law based on HCN observations, in addition to the SF law of atomic, molecular and total gas. In order to obtain the largest possible HCN sample, we compiled all well-sampled HCN measurements in local galaxies available in the literature.

In the work presented here, we scale the various gas components (atomic, molecular, total gas and dense molecular gas) and uniformly calibrated SFRs (either IR or RC) with the consistently derived radio sizes to derive the surface densities and their relations. A brief report of some preliminary results based on a smaller sam-

ple can be found in an earlier paper (Liu & Gao 2012). Here, we further increase our sample size by nearly 50% and present a thorough analysis and discussion. We describe our galaxy sample and data in § 2, and describe the method to measure galaxy sizes from radio maps in § 3. Our derivation and analysis of the global SF law in its various forms are presented in § 4. We discuss various related issues and factors that may have influence to the derived SF laws in § 5, and conclude in § 6. Throughout this paper, we adopt a flat cosmology with  $H_0 = 71 \text{ km s}^{-1} \text{ Mpc}^{-1}$  (Komatsu et al. 2011).

## 2. GALAXY SAMPLE AND DATA

### 2.1. Sample selection

Our sample is a combined sample of K98 and GS04b which contains 130 galaxies, supplemented by 51 additional sources with well-sampled HCN measurements available in the literature. K98 includes 61 spiral disk galaxies and 36 IR-selected starburst galaxies (circumnuclear IR starbursts in normal star forming galaxies and (U)LIRGs). GS04b contains 65 galaxies, of which  $\sim 25$  overlap with K98 sample. Finally, we excluded galaxies with known powerful active galactic nuclei (AGN) and galaxies with  $q$ -indices (Helou et al. 1985) less than 1.7. The final sample comprises 181 local galaxies, 66 of which are (U)LIRGs. It covers almost all morphological types, ranging from early types (E, S0) to late spirals and irregular galaxies. They are in a variety of environments, from apparently isolated galaxy to group or cluster members. The total-IR ( $8 - 1000 \mu\text{m}$ ) luminosity of our galaxies spans almost 5 orders of magnitude,  $\log(L_{\text{IR}}/L_{\odot}) \sim 7.8 - 12.3$ . The distances range from 0.75 to 280 Mpc. For each galaxy in the sample, we have high-resolution RC maps and integrated H I/CO/IR/RC fluxes. Of the entire sample of 181 galaxies, 128 galaxies have published HCN data in the literature, and 95 galaxies have published H I maps or H I sizes. Our sample is the largest sample of local star forming galaxies with H I/CO/HCN/IR/RC measurements available. All luminosities ( $L_{\text{HI}}$ ,  $L_{\text{CO}}$ ,  $L_{\text{HCN}}$ ,  $L_{\text{IR}}$  and  $L_{\text{RC}}$ ) and luminosity distances were converted to the common cosmological parameters adopted here.

### 2.2. Data

#### 2.2.1. H I data

H I maps or sizes for 95 of the 115 normal star forming galaxies in our sample were obtained from H I imaging surveys carried out with the (J)VLA and the Westerbork Synthesis Radio Telescope (WSRT). They are: (1) the H I Nearby Galaxy Survey (THINGS) (Walter et al. 2008), which provides high-resolution ( $FWHM \sim 6''$ ) VLA maps of nearby galaxies; (2) the VLA Imaging survey of Virgo galaxies in Atomic gas (VIVA) (Chung et al. 2009a), which includes H I images ( $FWHM \sim 15'' - 16''$ ) of late type galaxies in the Virgo cluster; (3) Local Irregulars That Trace Luminosity Extremes, The H I Nearby Galaxy Survey (Little THINGS) (Hunter et al. 2012), which assembles a dataset of high sensitivity and resolution ( $FWHM \sim 6''$ ) H I maps of dwarf irregular galaxies obtained with the (J)VLA; (4) the Westerbork H I Survey of Spiral and Irregular Galaxies (WHISP) (Swaters et al. 2002; Swaters & Balcells 2002; Noordermeer et al. 2005), a large H I survey of several hundreds of nearby spiral and

irregular galaxies ( $FWHM \sim 15'' \times 30''$ ); (5) the Westerbork SAURON H I Survey (Oosterloo et al. 2010), which presents deep H I maps for SAURON early-type galaxies ( $FWHM \sim 70'' \times 25''$ ).

The H I surface densities ( $\Sigma_{\text{HI}}$ ) for these 95 galaxies were derived in one of the following two ways. For 51 galaxies with H I maps publically available as fits files, we directly measured the average H I surface densities within our derived radio sizes (see § 3 for how we derived the radio sizes). For 44 of the galaxies, only published H I disk sizes (defined as where the face-on corrected H I surface density drops below  $1 M_{\odot} \text{ pc}^{-2}$ ) were available, we averaged the total H I mass over the H I sizes. We see no systematic differences in the H I surface densities between the two cases (see Fig. 2). Comparing the H I sizes with the radio sizes (see § 3) we found the former to be  $3 - 7 \times$  larger, which is not surprising since H I is often found to extend to the optical diameter of disk galaxies or even to larger scale lengths where star formation is not occurring (García-Ruiz et al. 2002; Swaters et al. 2002; Chung et al. 2009a). For the remaining 20 normal star forming galaxies no published H I maps or sizes were available, and we do not include them in our analysis of the  $\Sigma_{\text{SFR}} - \Sigma_{\text{HI}}$  relation.

We ignored the neutral atomic hydrogen in (U)LIRGs for the following reasons. First, the atomic gas fraction in (U)LIRGs is much smaller, and often negligible, compared with the molecular gas content, particularly within the compact starburst regions. It is well known that the  $\text{H}_2/\text{H I}$  ratio increases with the IR excess in (U)LIRGs (Mirabel & Sanders 1989) and active star forming spiral galaxies tend to have more than one order of magnitude higher  $\text{H}_2/\text{H I}$  ratio than those of the quiescent galaxies of extremely late Hubble types at lower luminosities (Young & Knezek 1989). Secondly, the H I distribution in (U)LIRGs often show complex morphologies, being distorted as the merger progresses (Hibbard et al. 2001b; Wang et al. 2001; Chen et al. 2002), or revealing elongated streams or tails of gas (e.g., Taramopoulos et al. 2001; Hibbard et al. 2001a). This also tends to clearly show some signatures in the global H I spectra in ULIRGs (e.g., van Driel et al. 2001). In addition, strong H I absorption feature is often seen against the nuclear regions of (U)LIRGs (Cole et al. 1999; Taramopoulos et al. 2001; Chen et al. 2002; Momjian et al. 2003).

### 2.2.2. CO data

Velocity-integrated CO fluxes were gathered from the literature and, when available, preference was given to CO fluxes derived directly from galaxy-integrated imaging measurements, of which we chose the values from single-dish maps (GS04b; Kuno et al. 2007; Chung et al. 2009b) over interferometer maps (Sofue et al. 2003; Helfer et al. 2003; Young et al. 2008) to avoid missing flux. Our second choice was the global CO fluxes inferred from observations along the major and/or minor axes of the disks, combining with model assumptions of the gas distribution (GS04b; Young et al. 1995; Paglione et al. 2001; Nishiyama & Nakai 2001). Instead of early CO surveys compiled in K98's work, which suffered from both small sample sizes and limited spatial coverage as well as sensitivity, the new CO surveys had made impressive progress in both sampled spatial coverage and observation resolution. The improved sensitivity

of these observation and facilities even allowed the cold molecular gas of early-type galaxies to be detected (e.g., Young et al. 2008; Crocker et al. 2011). We found a general agreement between the CO fluxes from the different surveys in the cases of overlapping CO measurements. The agreement is typically within 20% - 35%, although some interferometric fluxes deviated by as much as 20% - 50% from the single dish measurements. The data sets from surveys along major and/or minor axis deviated from single dish fluxes by smaller factors of 5% - 30%.

### 2.2.3. HCN data

We used the HCN (1-0) transition ( $n_{\text{crit}} \approx 1 \times 10^5 \text{ cm}^{-3}$ ) as a tracer of dense molecular gas, as it is one of the most abundant high dipole moment molecules and the most frequently observed interstellar molecules after CO in galaxies. In order to obtain the largest possible HCN (1-0) sample, we collected all robust measurements available in the literature. Our final HCN sample consists of 128 galaxies in total, mostly from GS04b, Baan et al. (2008), and García-Burillo et al. (2012). It also includes recent HCN (1-0) detections of a handful of CO-luminous early-type galaxies (Krips et al. 2010; Crocker et al. 2012), which enabled us to probe the dense gas SF law at lower luminosities. The compiled sample spanned 3 orders in HCN luminosity ( $L'_{\text{HCN}}/(\text{K km s}^{-1} \text{ pc}^2) \sim 10^{7.1-9.7}$ ). It consists of 65 (U)LIRGs, 47 spiral galaxies, and 16 early-type galaxies. The formulas to calculate atomic gas mass, molecular mass, and dense molecular mass from the observed line fluxes are given in Appendix A.

### 2.2.4. IR and 1.4 GHz RC data

The IR emission is a sensitive tracer of the young stellar population and SFR, as a significant fraction of the bolometric luminosity of a galaxy is absorbed by interstellar dust and re-emitted in the thermal IR (K98). Total-IR  $8 - 1000 \mu\text{m}$  luminosities were calculated using 12, 25, 60, 100  $\mu\text{m}$  photometry from the *Infrared Astronomical Satellite* (IRAS) and the formulas presented in Table 1 of Sanders & Mirabel (1996).

The 1.4 GHz radio continuum emission probes synchrotron radiation from supernovae remnants and thermal emission from H II regions, whose progenitors are both short-lived massive stars and hence trace recent SF (e.g., Condon 1992; Yun et al. 2001). This make the radio a reliable tracer of SF, as indicated by the tight IR-radio correlation. Integrated 1.4 GHz radio fluxes were, for the most part, obtained from the NRAO VLA Sky Survey (NVSS; Condon et al. 1998; Yun et al. 2001; Condon et al. 2002). Due to its large beam size and high sensitivity, the NVSS is able to provide reliable integrated flux measurements. For the remaining sources, 1.4 GHz fluxes were obtained from a number of other radio surveys, see Table 1 for references. Mono-chromatic (1.4 GHz) radio luminosities were subsequently inferred using  $L_{1.4\text{GHz}} = 4\pi D_L^2 S_{1.4\text{GHz}}$ . Table 1 lists the distance, as well as CO, HCN, IR and RC luminosities.

## 3. RADIO SIZES AND STAR FORMATION RATES

We do not only use integrated radio (1.4 GHz) fluxes to trace SFRs of galaxies, but also utilize radio images to derive the sizes of star forming regions. About two

thirds of our sources had published high-resolution radio maps from various systematic VLA radio imaging surveys (Condon 1987; Condon et al. 1990, 1991, 1996; Becker et al. 2003). The remaining one third ( $\sim 64$  sources) did not however, (or in some cases they were of poor quality), and in those cases we had to reduce the raw data retrieved from the NRAO archive (<https://archive.nrao.edu>) using *AIPS*. The image reduction was done using standard *AIPS* procedures, i.e. blanking of bad visibilities, followed by calibration and CLEAN imaging. In some cases, data sets from different VLA configurations were combined in the visibility plane to improve sensitivity and resolution. This step was done using the task DBCON after each *uv* data set had been calibrated separately. For a few ( $\sim 3$ ) southern sources, radio maps from the Molonglo Observatory Synthesis Telescope (MOST) were used (Mauch et al. 2008). As a consistency check, we compared the NVSS radio fluxes with the integrated fluxes derived from our reduced maps and found good agreement.

The typical noise level of our radio maps is  $\sim 0.1$  mJy beam $^{-1}$ , which should be sufficient to detect low-brightness emission and allow for accurate measurement of the radio size. Radio sizes were determined from 2D Gaussian fits in the image plane using the *AIPS* task IMFIT. A detailed description of the radio size measurements and related issues, such as AGN contamination and missing flux problem due to high-resolution interferometer data, are given in the Appendix B.

The radio size may arguably serve as a more truthful picture of the extent of the star forming regions than the mixture of IR and CO maps often used, since the radio continuum is a well-known, extinction-free SF tracer (Condon et al. 1991, 1996) while both of IR and CO observations often suffer from very limited sensitivity and resolution. Furthermore, in some cases CO may also be tracing diffuse molecular gas that is not actively forming stars (Bothwell et al. 2010; Rujopakarn et al. 2011), while the IR emission have a significant contribution from dust heated by the ambient FUV field from evolved stellar population. The radio continuum, on the other hand, probes synchrotron radiation from supernovae remnants and thermal emission from H II regions, both of which have short-lived massive stars as progenitors, and may therefore be a better tracer of the recent SF and its spatial extent within galaxies.

Sizes inferred from optical images, often adopted for normal galaxies, include old stellar components that usually extend beyond the regions where the SF is occurring. Indeed, a comparison of the optical sizes of the normal galaxies from K98 with our measured radio sizes shows the former to be  $2 - 5\times$  larger, with an average value of  $\sim 3.3$ . The approach of utilizing radio continuum maps provides a more uniform way to determine the SFRs as well as the sizes of the actively star forming regions for a variety galaxy types.

The ideal way to derive disk-averaged surface densities of molecular and dense molecular gas is to measure them directly from CO and HCN maps. Unfortunately, this is impractical for large sample of galaxies at the moment owing to the limited sensitivity and weakness of HCN emission. The strategy adopted here is to use our measured RC sizes as an estimate of the spatial extent of the molecular gas as well. This is a reasonable as-

sumption since CO and HCN are known to trace SF in our own Galaxy (Wu et al. 2005) and in external galaxies (Murgia et al. 2002; Iono et al. 2009), and so should be tightly correlated with RC which is itself a tracer of ongoing formation of massive stars (Liu & Gao 2010). Indeed, morphological similarities between RC and the molecular gas has not only been found in normal spiral galaxies (Crosthwaite et al. 2002; Schuster et al. 2007) and (U)LIRGs (Condon et al. 1991; Downes & Solomon 1998; Murgia et al. 2005; Tacconi et al. 2006), but also in early type galaxies (Lucero & Young 2007).

Comparing the radio sizes of a subsample of 81 galaxies with their CO sizes collected from the literature, a quite good agreement was found (Fig. 1). CO sizes differ from RC sizes within a factor  $\sim 2 - 3$ , with an average ratio of  $\sim 1.1$ . The CO sizes were derived from: (1) interferometry measurements (e.g., Bryant & Scoville 1999; Regan et al. 2001; Iono et al. 2009); (2) single-dish maps (e.g., Leroy et al. 2009; Chung et al. 2009b); (3) the observations along the major and/or minor axes of the disks (e.g., Young et al. 1995) in literature. The good correlation between RC size and CO size indicates that the RC traces the global CO emission reasonably well. However, we notice that the CO sizes seem to be systematically larger than the RC sizes at the low end (Fig. 1) which could be due to CO also tracing diffuse non-SF gas as suggested above. In extremely compact starbursts, the typical size scale of SF is much smaller than  $\sim 1$  kpc.

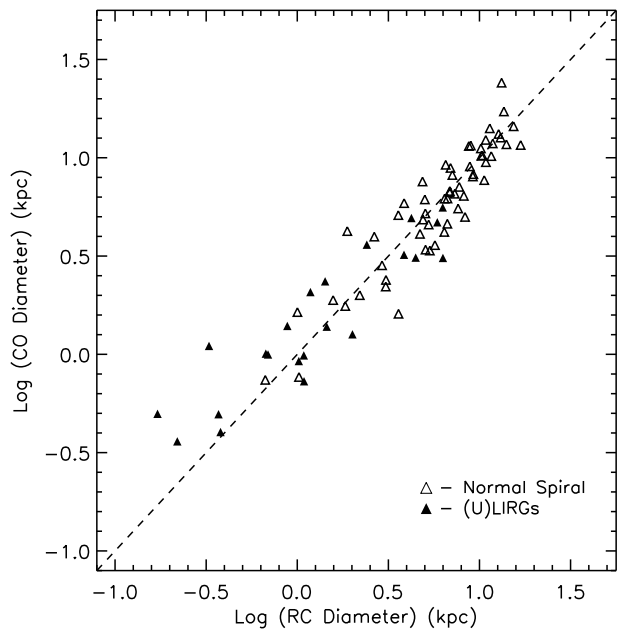


FIG. 1.— CO size vs. RC size for 81 galaxies in our sample. The distribution of CO and RC sizes generally scale linearly (dashed line). This indicates that the RC and CO emission generally trace each other well. The sizes of normal disk galaxies span a range of  $\sim 1 - 15$  kpc, while ULIRGs are much more compact with size  $\leq 1.5$  kpc. At the low end, the CO sizes seem to be systematically larger than the RC sizes, suggesting CO could also trace diffuse molecular gas that is not actively forming stars.

The SFRs were inferred in two independent ways, namely from the IR luminosities and the rest-frame 1.4 GHz luminosities derived in § 2.2.4. To this end we adopted the luminosity-SFR calibrations provided by Bell (2003) which account for the reduced effi-

ciency of IR and radio emission in low-luminosity galaxies (i.e., the IR and radio emission underestimate the SFRs of low-luminosity galaxies) (Price & Duric 1992; Wang & Heckman 1996). We describe the detailed formulas for calculating SFRs in Appendix A.4. Overall, the IR- and RC-based SFRs were in agreement (see Appendix A.4 for details) and we shall use the IR-based values in the following. But some examples of SF laws derived by adopting RC-based SFRs were given in Appendix A.4. The resulting deconvolved major axes, as well as surface densities for atomic gas, molecular gas, total gas, dense molecular gas and IR/RC-based SFRs are given in Table 2.

#### 4. RESULTS

The surface densities of molecular, total gas, dense molecular gas and SFRs are derived by the formula  $\Sigma = \frac{\text{Integrated Value}}{2\pi r_{\text{RC}}^2}$ , where  $r_{\text{RC}}$  is the deconvolved HWHM along the major axis of the RC maps (see Table 2) to account for the galaxy inclination to first order. The factor 1/2 is introduced to provide a better estimate of observed surface densities over galaxies.

A realistic estimate of the uncertainty on the observed CO/HCN/IR/RC fluxes is  $\sim 30\%$ . However, considering the additional uncertainties in the calibrations that convert observed fluxes to physical quantities (i.e., luminosities, SFRs, and gas masses) as well as measurement errors in radio sizes, we adopted a systematic uncertainty of 50% (i.e., 0.22 dex) on the final surface densities of SFR and gas. To compute the linear regression between surface densities of SFRs and gas we used the publicly available Bayesian Markov Chain Monte Carlo (MCMC) IDL routine `linmix_err` (Kelly 2007), which accounts for measurement errors in the x and y variables, upper limits and intrinsic scatters.

We fit our SF laws with three parameters: power-law index  $N$ , normalization  $A$  and intrinsic scatter  $\epsilon$ . The functional form is:  $\log \Sigma_{\text{SFR}} = N \log \Sigma_{\text{gas}} + A + \mathcal{N}(0, \epsilon)$ , where  $\mathcal{N}(0, \epsilon)$  is introduced as a logarithmic deviation from the power law, drawn from a normal distribution with zero mean and standard deviation  $\epsilon$ . The intrinsic scatter  $\epsilon$  is caused by genuine differences in the SF properties of our galaxies, yet the conservative systematic errors (50%) adopted prevent us from extracting this information (i.e., the fit returns  $\epsilon \sim 0$ ).

For the sake of convenience we shall refer to “surface density” as “density” for the remainder of the paper.

##### 4.1. $\Sigma_{\text{HI}}$ vs. $\Sigma_{\text{SFR}}$

Fig. 2 shows the distribution of  $\Sigma_{\text{SFR}}$  versus  $\Sigma_{\text{HI}}$  for the 95 normal disk galaxies with HI density measurements from 21 cm maps (see § 2.2.1). We find there is no correlation between the globally averaged densities of SFRs and HI in disk galaxies. The values of  $\Sigma_{\text{HI}}$  stays within a fairly small range ( $\leq 2$  dex), while  $\Sigma_{\text{SFR}}$  spans more than 4 orders of magnitude ( $\sim 5$  dex).

Another feature in Fig. 2 is that the HI density saturates at a maximum value of about  $25 M_{\odot} \text{ pc}^{-2}$  (indicated by the dashed line). A similar cutoff in HI density was also seen in the studies on spatially resolved SF law (Wong & Blitz 2002; Kennicutt et al. 2007; Bigiel et al. 2008). The saturation in HI density may indicate a transition from atomic to molecular gas where at increasing

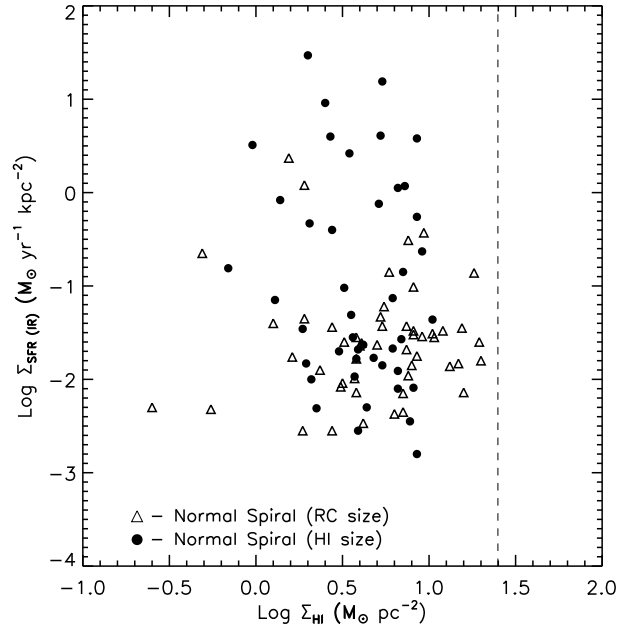


FIG. 2.—  $\Sigma_{\text{SFR}}$  vs.  $\Sigma_{\text{HI}}$  for the 95 normal disk galaxies with HI measurements. Filled circles indicate galaxies for which  $\Sigma_{\text{HI}}$  was derived by averaging total HI mass over HI size, while triangles show galaxies where  $\Sigma_{\text{HI}}$  was determined by averaging HI mass within the RC size (see § 2.2.1). The plot shows no correlation between  $\Sigma_{\text{SFR}}$  and  $\Sigma_{\text{HI}}$ . The dashed line indicates the maximum HI surface density of  $25 M_{\odot} \text{ pc}^{-2}$  found in our sample.

column densities, the cold atomic gas harbors regions that are able to self-shield against photo-dissociation by the interstellar radiation field (ISRF) and thus allow  $\text{H}_2$  to form (Krumholz et al. 2008, 2009).

#### 4.2. $\Sigma_{\text{H}_2}$ vs. $\Sigma_{\text{SFR}}$

##### 4.2.1. Fixed $\alpha_{\text{CO}}$

Fig. 3 (a) shows the relation between  $\Sigma_{\text{SFR}}$  and  $\Sigma_{\text{H}_2}$  on a logarithmic scale for all galaxies in our sample, where a fixed Galactic CO-to- $\text{H}_2$  conversion factor ( $\alpha_{\text{CO}}$ ) value of  $4.6 M_{\odot} (\text{K km s}^{-1} \text{ pc}^2)^{-1}$  was adopted (Young & Scoville 1991). Taken together, the normal disks and (U)LIRGs span a dynamic range of approximately  $10^6$  in SFR and molecular gas densities. There is a strong correlation between  $\Sigma_{\text{SFR}}$  and  $\Sigma_{\text{H}_2}$  and a Spearman rank correlation test gives a correlation coefficient of 0.96. Fitting the power law relation using `linmix_err` to the data (with associated uncertainties of 50%) yields  $N = 1.14 \pm 0.02$  and  $A = -3.16 \pm 0.06$  (solid line in Fig. 3 (a)). The rms scatter of the data around this best-fit line is  $\sim 0.40$  dex. Fitting to disk galaxies and (U)LIRGs separately yields slopes of  $N = 0.97 \pm 0.04$  and  $N = 1.12 \pm 0.04$ , respectively. The scatter of the data around these best fit lines is significantly larger for the disk galaxies ( $\sim 0.41$  dex) than for the (U)LIRGs ( $\sim 0.22$  dex). This is partly due to the shallower  $\Sigma_{\text{SFR}} - \Sigma_{\text{H}_2}$  relation at low densities, where the (formal)  $\Sigma_{\text{SFR}}\text{-to-}\Sigma_{\text{H}_2}$  ratios exceed that expected from the best fit.

##### 4.2.2. Varying $\alpha_{\text{CO}}$

In the following, we examine the SF law obtained when adopting a varying, rather than a fixed, CO-to- $\text{H}_2$  conversion factor. Our first approach is to adopt a conversion factor of  $0.8 M_{\odot} (\text{K km s}^{-1} \text{ pc}^2)^{-1}$  for (U)LIRGs

(Downes & Solomon 1998), but maintaining the Galactic value for normal disk galaxies. As a result, normal galaxies and (U)LIRGs split up into two distinct  $\Sigma_{\text{SFR}}$  vs.  $\Sigma_{\text{H}_2}$  relations as shown in Fig. 3 (b). The fitted slopes for each sub-sample, i.e., normal galaxies and (U)LIRGs, do not change, but the normalization ( $A$ ) for (U)LIRGs increases by  $\sim 0.8$  dex, indicating the increased SF efficiencies in these systems.

Our second approach is to adopt continuously varying  $\alpha_{\text{CO}}$ -values based on the modeling results by Narayanan et al. (2012) who parametrizes  $\alpha_{\text{CO}}$  as a function of CO line intensity and metallicity (see their eq. 11). Assuming a constant metallicity  $Z = 1$  for all our galaxies, we found  $\alpha_{\text{CO}}$  values in the range  $3.5 - 6.3 M_{\odot} (\text{K km s}^{-1} \text{pc}^2)^{-1}$  for the low-luminosity galaxies,  $2.0 - 5.0 M_{\odot} (\text{K km s}^{-1} \text{pc}^2)^{-1}$  for normal spirals and  $0.3 - 3.0 M_{\odot} (\text{K km s}^{-1} \text{pc}^2)^{-1}$  for (U)LIRGs. The resulting  $\Sigma_{\text{SFR}}-\Sigma_{\text{H}_2}$  relation is shown in Fig. 3 (c) and is seen to be significantly steeper ( $N \simeq 1.6$ ) compared to the relations in Fig. 3 (a) and (b). A best-fit power-law to the full sample yields a unimodal  $\Sigma_{\text{SFR}}-\Sigma_{\text{H}_2}$  relation of the form:  $\log \Sigma_{\text{SFR}} = (1.60 \pm 0.03) \log \Sigma_{\text{H}_2} - (4.11 \pm 0.09)$ .

#### 4.3. $\Sigma_{\text{gas}}$ vs. $\Sigma_{\text{SFR}}$

The total gas density  $\Sigma_{\text{gas}}$  is the sum of atomic gas density  $\Sigma_{\text{HI}}$  and molecular gas density  $\Sigma_{\text{H}_2}$ . When  $\Sigma_{\text{HI}}$  data were unavailable (which was the case for a few normal galaxies), we took  $\Sigma_{\text{H}_2}$  as a lower limit on  $\Sigma_{\text{gas}}$ . For (U)LIRGs, the atomic gas content is often negligible compared with the molecular gas, and we set  $\Sigma_{\text{gas}} \simeq \Sigma_{\text{H}_2}$ . Fig. 4 (a-c) shows  $\Sigma_{\text{SFR}}$  vs.  $\Sigma_{\text{gas}}$ , where a uniform, bimodal and continuous  $\alpha_{\text{CO}}$  has been adopted, respectively.

We derive the following best-fits to the data:

uniform  $\alpha_{\text{CO}}$ :

$$\Sigma_{\text{SFR}} = 10^{-3.56 \pm 0.06} \Sigma_{\text{gas}}^{1.24 \pm 0.02} \quad (\text{disks} + (\text{U})\text{LIRGs})(1)$$

bi-modal  $\alpha_{\text{CO}}$ :

$$\Sigma_{\text{SFR}} = 10^{-3.46 \pm 0.09} \Sigma_{\text{gas}}^{1.15 \pm 0.04} \quad (\text{disks}) \quad (2)$$

$$\Sigma_{\text{SFR}} = 10^{-2.12 \pm 0.13} \Sigma_{\text{gas}}^{1.12 \pm 0.04} \quad ((\text{U})\text{LIRGs}) \quad (3)$$

$$\Sigma_{\text{SFR}} = 10^{-3.73 \pm 0.11} \Sigma_{\text{gas}}^{1.46 \pm 0.04} \quad (\text{disks} + (\text{U})\text{LIRGs})(4)$$

continuous  $\alpha_{\text{CO}}$ :

$$\Sigma_{\text{SFR}} = 10^{-4.61 \pm 0.09} \Sigma_{\text{gas}}^{1.75 \pm 0.03} \quad (\text{disks} + (\text{U})\text{LIRGs})(5)$$

The scatter of the data around the above best-fit relations are  $\sim 0.36$  dex,  $\sim 0.62$  dex (disks+(U)LIRGs), and  $\sim 0.43$  dex, respectively.

The  $\Sigma_{\text{SFR}}$  is a steeper function of total gas density  $\Sigma_{\text{gas}}$  than that of molecular gas density  $\Sigma_{\text{H}_2}$ . This is mainly owing to the increasing fraction of atomic gas towards lower luminosity galaxies. At the high density end (mostly populated by molecular-rich spirals and (U)LIRGs), the ISM is largely molecular and  $\Sigma_{\text{SFR}}-\Sigma_{\text{gas}}$  essentially follows the  $\Sigma_{\text{SFR}}-\Sigma_{\text{H}_2}$  relation.

#### 4.4. $\Sigma_{\text{dense}}$ vs. $\Sigma_{\text{SFR}}$

Fig. 5 shows  $\Sigma_{\text{SFR}}$  vs.  $\Sigma_{\text{dense}}$ , where  $\Sigma_{\text{dense}}$  was derived for our compiled HCN sample of 128 galaxies adopting a constant Galactic HCN  $\rightarrow$   $M_{\text{dense}}$  conversion factor ( $\alpha_{\text{HCN}}^{\text{MW}}$ ) value of  $10 M_{\odot} (\text{K km s}^{-1} \text{pc}^2)^{-1}$ . One can

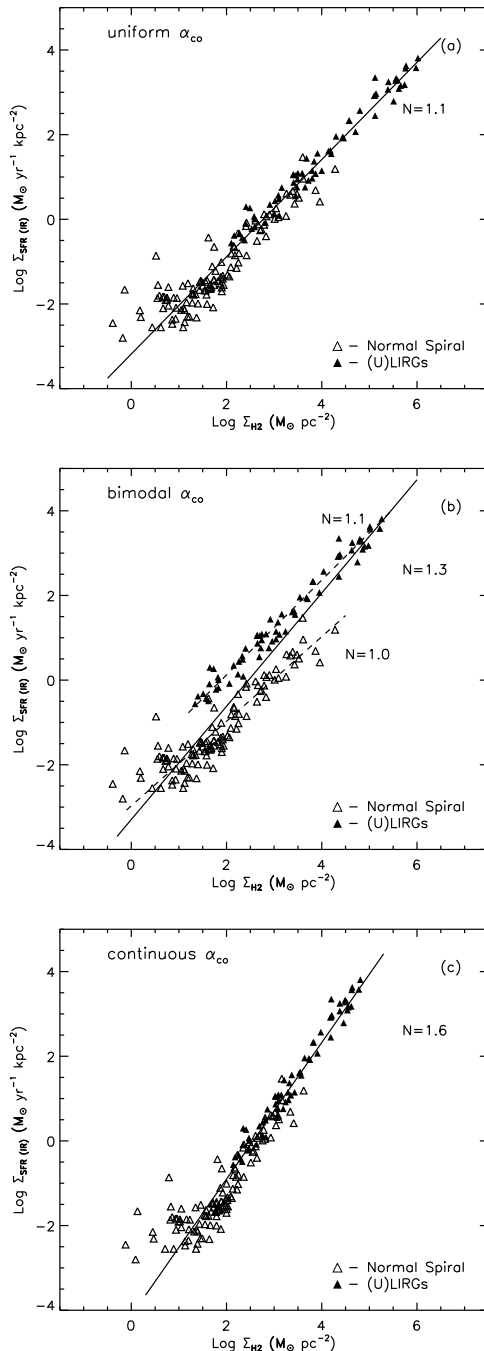


FIG. 3.—  $\Sigma_{\text{SFR}}$  vs.  $\Sigma_{\text{H}_2}$  in the cases where (a) a single (Galactic)  $\alpha_{\text{CO}}=4.6$  value has been applied to the entire sample; (b) separate values of  $\alpha_{\text{CO}} = 4.6$  and  $0.8$  were applied to disk and (U)LIRGs, respectively, and (c) a continuously varying  $\alpha_{\text{CO}}$  was applied.

clearly see a very tight  $\Sigma_{\text{SFR}}-\Sigma_{\text{dense}}$  correlation spanning more than  $\sim 6$  orders of magnitude in density and we find a best-fit log-linear relation of:

$$\log \Sigma_{\text{SFR}} = (1.01 \pm 0.02) \log \Sigma_{\text{dense}} - (1.82 \pm 0.05). \quad (6)$$

A Spearman rank correlation test yields a correlation coefficient of  $\sim 0.99$ . The dispersion in the  $\Sigma_{\text{SFR}}-\Sigma_{\text{dense}}$  relation ( $\sim 0.32$  dex) is smaller than the relations between densities of SFRs and other gas components (atomic, molecular, and total gas).

We find a linear SF law ( $N = 1.01 \pm 0.02$ ) in terms of

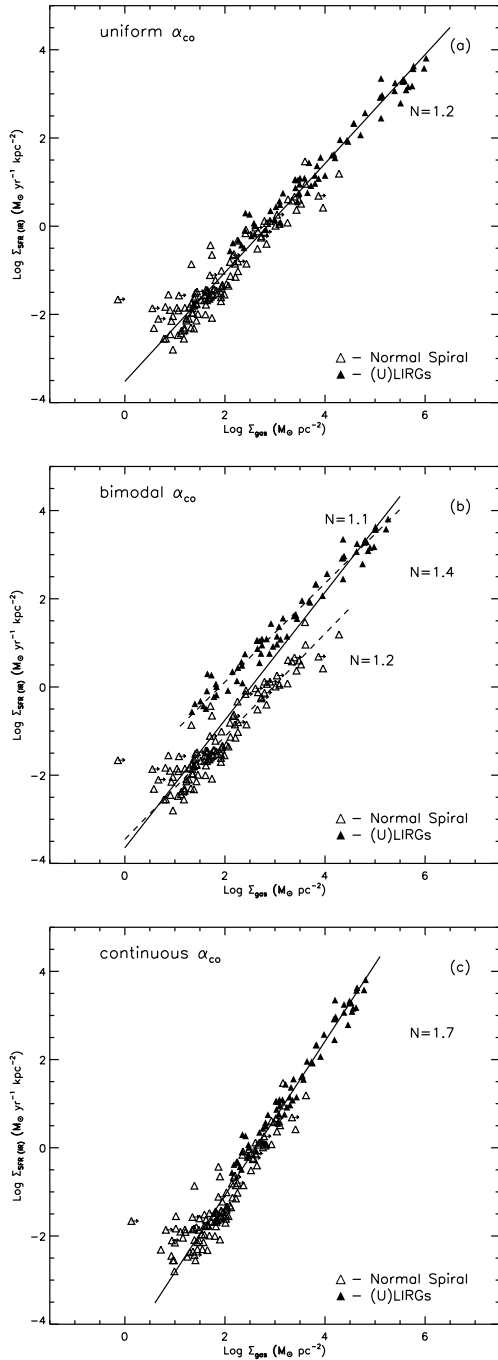


FIG. 4.—  $\Sigma_{\text{SFR}}$  vs.  $\Sigma_{\text{gas}}$  in the cases where (a) a single (Galactic)  $\alpha_{\text{CO}}=4.6$  value has been applied to the entire sample; (b) separate values of  $\alpha_{\text{CO}} = 4.6$  and  $0.8$  were applied to disk and (U)LIRGs, respectively, and (c) a continuously varying  $\alpha_{\text{CO}}$  was applied. We took values of  $\Sigma_{\text{H}_2}$  as lower limits on  $\Sigma_{\text{gas}}$  in the cases where  $\Sigma_{\text{H}_1}$  were unavailable. The  $\Sigma_{\text{SFR}}-\Sigma_{\text{gas}}$  relations generally follow the  $\Sigma_{\text{SFR}}-\Sigma_{\text{H}_2}$  relations, but exhibiting steeper slopes.

dense molecular gas, in agreement with the tight linear relation found between  $L_{\text{IR}}$  and  $L_{\text{HCN}}$  (GS04a,b). Scaling the dense molecular gas mass and SFRs by our measured RC disk sizes does not change the slope of the  $L_{\text{IR}}-L_{\text{HCN}}$  correlation since this relation is essentially exactly linear.

Fitting to spiral galaxies and (U)LIRGs separately (each constituting about half of the HCN sample), we derive identical  $\Sigma_{\text{SFR}}-\Sigma_{\text{dense}}$  relations within the errors, both in terms of the slope ( $N$ ) and the overall normal-

ization ( $A$ ):  $N = 0.98 \pm 0.05$  ( $N = 0.96 \pm 0.04$ ) and  $A = -1.84 \pm 0.06$  ( $A = -1.57 \pm 0.10$ ) for normal spirals ((U)LIRGs).

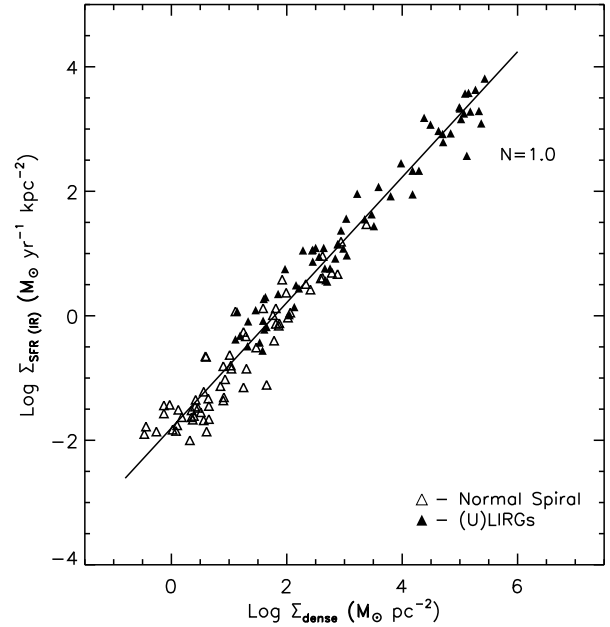


FIG. 5.—  $\Sigma_{\text{dense}}$  vs.  $\Sigma_{\text{SFR}}$  for our sample. The  $\Sigma_{\text{dense}}-\Sigma_{\text{SFR}}$  relation is the tightest one among all correlations, and it is linear ( $N=1.01 \pm 0.02$ ). Fitting to normal galaxies and (U)LIRGs separately yields identical linear correlation within the uncertainties.

So far, we have only presented the results of the various SF laws related to IR-based SFRs. As mentioned above, we derived our SFRs in two independent ways using both IR and RC data. Excellent agreement were found between the two SFRs estimators, and using one over the other, therefore, did not alter our results in any significant way. Further details on the various SF laws related to RC-based SFRs are given in the Appendix A.4.

## 5. DISCUSSION

### 5.1. Deviations from the molecular gas SF law

An interesting finding in our global  $\Sigma_{\text{SFR}}-\Sigma_{\text{H}_2}$  relation is the higher IR-to-CO ratios exhibited by less massive, low-luminosity galaxies compared with normal spirals (Fig. 3). These galaxies have  $\Sigma_{\text{H}_2} \leq 10 M_{\odot} \text{ yr}^{-1}$  and deviate significantly from the derived  $\Sigma_{\text{SFR}}-\Sigma_{\text{H}_2}$  relations for whole sample (see solid lines in Fig. 3). These low-luminosity galaxies are usually atomic gas dominated and metal-poor (Sadler et al. 2000; Sadler 2001). The higher IR-to-CO ratios in these galaxies may be due to systematic underestimates of their total molecular gas mass as the adopted  $\alpha_{\text{CO}}$  are too small for these systems. In low-metallicity environments, photodissociation destroys CO more easily, whereas the  $\text{H}_2$  can self-shield more effectively (Narayanan et al. 2012) so that the  $\alpha_{\text{CO}}$  tends to be larger than the Galactic value and increases with decreasing metallicity and dust-to-gas ratio (e.g., Boselli et al. 2002; Leroy et al. 2011; Krumholz et al. 2011; Rahman et al. 2012; Bolatto et al. 2011, 2013). Although a continuously varying  $\alpha_{\text{CO}}$  was introduced in our analysis, as we assumed constant metallicity  $Z = 1$  (§ 4.2.2) we could still underestimate their molecular gas mass.

Alternatively, we note that, some low-luminosity galaxies may indeed exhibit higher SFE than large spiral galaxies (Gardan et al. 2007; Gratier et al. 2010; Schrubba et al. 2011; Saintonge et al. 2012; Leroy et al. 2013). Minor starburst events in these systems (Saintonge et al. 2012), or suppression of SF in large spiral galaxies by dynamical effects (Leroy et al. 2013), are possible explanations.

At the high density end of Fig. 3, where mostly (U)LIRGs (mergers) reside, the molecular SFE goes up again as the plot turns steeper in these regimes. In these galaxy mergers, the observed  $\alpha_{\text{CO}}$  are suggested to be much lower (by a typical factor of  $\sim 2 - 10$ ) than the normal galaxies because the rise in velocity dispersion and kinetic temperature in GMCs during the merger increases the CO intensity (Narayanan et al. 2011). The  $\Sigma_{\text{SFR}} - \Sigma_{\text{H}_2}$  relation derived by using bimodal  $\alpha_{\text{CO}}$  clearly display the higher  $\Sigma_{\text{SFR}}\text{-to-}\Sigma_{\text{H}_2}$  ratios of (U)LIRGs than that of normal spirals, showing two distinct regimes, one for normal galaxies and one for starbursts (see Fig. 3 (b)). It appears to be similar to the bi-modal relations found from high- $z$  CO observations, where two different  $\alpha_{\text{CO}}$  conversion factors were used (Daddi et al. 2010; Genzel et al. 2010; Ivison et al. 2011; Riechers 2012).

The trend that (U)LIRGs have higher molecular SFE is even more obvious as a continuously varying  $\alpha_{\text{CO}}$  was adopted. We found a unimodal  $\Sigma_{\text{SFR}}\text{-}\Sigma_{\text{H}_2}$  relation with a clearly super-linear power-law index ( $N = 1.60 \pm 0.03$ , see Fig. 3 (c)). It is worth noting here that a metallicity dependence would further steepen this fit. We noticed that this power law relation is comparable to that derived by Bouché et al. (2007) which obtained a universal SF law for a sample of local and high- $z$  galaxies ( $\log \Sigma_{\text{SFR}} = (1.7 \pm 0.05) \log \Sigma_{\text{H}_2} + (-4.03 \pm 0.10)$ ). We tend to believe that  $\alpha_{\text{CO}}$  varies continuously rather than in a bi-model way because there should be no clear boundary between starbursts and disk spirals. Our RC images show that some normal galaxies exhibit strong compact starburst regions in the center which are comparable to many LIRGs (such as NGC253, NGC1097 and NGC3504). As a consequence, the derived densities for disk galaxies and (U)LIRGs show an overlapping region up to two orders of magnitude (see Fig. 3 & Fig. 4). It is thus natural to expect the  $\alpha_{\text{CO}}$  varies continuously from normal disks to (U)LIRGs as well. A super-linear power law index of  $\sim 1.6$  derived here suggested a density-dependent SFE.

Although the result is sensitive to the  $\alpha_{\text{CO}}$  conversion factor, we still get a general picture of SF law in molecular gas: in disk galaxies with  $10 < \Sigma_{\text{H}_2} < 100 \text{ M}_\odot \text{ pc}^{-2}$ , where molecular gas dominates and is gravitationally bound to GMCs with approximately uniform properties, the  $\Sigma_{\text{SFR}}$  is roughly linear proportional to  $\Sigma_{\text{H}_2}$ . The value of  $\Sigma_{\text{H}_2} \sim 100 \text{ M}_\odot \text{ pc}^{-2}$  is the characteristic density of individual giant molecular clouds (GMCs). In starburst galaxies (mostly (U)LIRGs) with  $\Sigma_{\text{H}_2} > 100 \text{ M}_\odot \text{ pc}^{-2}$ , where supersonic turbulence is known to be a dominant process controlling SF, the  $\Sigma_{\text{SFR}}\text{-}\Sigma_{\text{H}_2}$  relation appears considerably steeper than linear, implying an increasing molecular SFE. In low-luminosity galaxies with  $\Sigma_{\text{H}_2} < 10 \text{ M}_\odot \text{ pc}^{-2}$ , where atomic gas dominates ISM, the  $\Sigma_{\text{SFR}}\text{-}\Sigma_{\text{H}_2}$  relation show visibly increasing galaxy-to-galaxy scatter and higher IR-to-CO ratios.

## 5.2. The role of atomic gas and SF law for total gas

We found there is no correlation between  $\Sigma_{\text{SFR}}$  and  $\Sigma_{\text{HI}}$  (see Fig. 2). We can even see the discrepancy between the morphologies of SFR and atomic gas from RC maps and HI maps, that some galaxies show central HI depressions where significant SF is still occurring. More detailed studies on local scales showed little or no correlation between  $\Sigma_{\text{SFR}}$  and  $\Sigma_{\text{HI}}$  as well (Wong & Blitz 2002; Kennicutt et al. 2007; Bigiel et al. 2008).

The HI saturation value of  $\sim 25 \text{ M}_\odot \text{ pc}^{-2}$  found in our study coincides with the maximum HI value derived from Kennicutt et al. (2007) studying the spatially resolved SF law in M51 on  $\sim 500 \text{ pc}$  scale, but is higher than the value of  $\sim 10 \text{ M}_\odot \text{ pc}^{-2}$  found by Wong & Blitz (2002) and Bigiel et al. (2008). We supposed this may due to the larger range of metallicity in our sample, given the result by theoretical modeling that the characteristic column density of the transition from atomic to molecular gas increases with metallicity, and is around  $\sim 10 \text{ M}_\odot \text{ pc}^{-2}$  at solar metallicity (Krumholz et al. 2009).

Although atomic gas itself shows no correlation with SFR, but it still plays important role in regulating the SF law of total gas. The combined density of atomic and molecular gas, i.e., the total gas density  $\Sigma_{\text{gas}}$ , shows a steeper function with  $\Sigma_{\text{SFR}}$  than molecular gas density  $\Sigma_{\text{H}_2}$ . This is mainly due to the increasing fraction of atomic gas towards lower luminosity galaxies. An interesting question is whether total gas density  $\Sigma_{\text{gas}}$  or molecular gas density  $\Sigma_{\text{H}_2}$  correlates better with the star formation  $\Sigma_{\text{SFR}}$ . That is which of the  $\Sigma_{\text{SFR}} - \Sigma_{\text{H}_2}$  and  $\Sigma_{\text{SFR}} - \Sigma_{\text{gas}}$  relations might be more fundamental. Some works asserted that the good correlation between  $\Sigma_{\text{SFR}}$  and  $\Sigma_{\text{gas}}$  is driven by the molecular gas SF law and the ratio of molecular to atomic hydrogen (Wong & Blitz 2002; Bigiel et al. 2008; Blanc et al. 2009). In this picture, molecular clouds are first formed from HI, and stars are then formed exclusively from molecular gas. On the contrary, some other works claimed that it is the gas phases as a whole feeds the SF activity. Where the gas is predominantly molecular in most of spiral galaxies and (U)LIRGs, the correlation of  $\Sigma_{\text{SFR}}$  with  $\Sigma_{\text{H}_2}$  could be only a manifestation of the underlying correlation of the  $\Sigma_{\text{SFR}}$  with  $\Sigma_{\text{gas}}$  (Kennicutt et al. 2007; Fumagalli et al. 2009). Our work shows that at the density regimes with  $\Sigma_{\text{H}_2} > 10 \text{ M}_\odot \text{ pc}^{-2}$ , the  $\Sigma_{\text{SFR}}$  correlates equally well with total gas  $\Sigma_{\text{gas}}$  and molecular gas  $\Sigma_{\text{H}_2}$ . While at the low density regime where  $\Sigma_{\text{H}_2} < 10 \text{ M}_\odot \text{ pc}^{-2}$ , we can see that the scatter in the  $\Sigma_{\text{SFR}} - \Sigma_{\text{gas}}$  relation is significantly smaller (with scatter  $\sim 0.43$  dex, see Fig. 3) than that in the  $\Sigma_{\text{SFR}} - \Sigma_{\text{H}_2}$  relation (with scatter  $\sim 0.55$  dex, see Fig. 4). This may indicate that there could be some other parameter apart from the molecular gas content that determines the SFRs for galaxies, at least in low-luminosity galaxies, and atomic gas may have indirect effect on SF.

Several investigations of the total gas SF law have found a threshold in the gas surface density ( $\Sigma_{\text{gas}} \sim 5 - 10 \text{ M}_\odot \text{ pc}^{-2}$ ) below which the SFR declines rapidly and SF is strongly suppressed (Kennicutt 1998; Martin & Kennicutt 2001; Leroy et al. 2005; Kennicutt 2008). These thresholds are mostly observed in galaxies like dwarf galaxies and low surface brightness (LSB)

galaxies (Leroy et al. 2005; Wyder et al. 2009). As most of our galaxies have total gas density larger than the characteristic threshold value of  $\sim 10 M_{\odot} \text{pc}^{-2}$  (with less than 10 galaxies having  $\Sigma_{\text{SFR}}$  under this value), we do not find a clear threshold in our sample.

### 5.3. SFRs vs dense gas

The tightest relation (with scatter of  $\sim 0.32$  dex) in our results is the linear relation between  $\Sigma_{\text{SFR}}$  and  $\Sigma_{\text{dense}}$ . We fit the normal galaxies and (U)LIRGs separately and find both the power indices are close to unity. Therefore, the tight linear correlation between  $\Sigma_{\text{dense}}$  and  $\Sigma_{\text{SFR}}$  is established within the whole sample of galaxies, independent of IR luminosity.

In contrast, García-Burillo et al. (2012) suggested a two-function power law in terms of dense molecular gas SF law, which claimed a higher slope in (U)LIRGs ( $1.05 \pm 0.05$ ) than normal galaxies ( $0.90 \pm 0.06$ ). We noticed that García-Burillo et al. (2012) adopted a bi-modal HCN-to- $M_{\text{dense}}$  conversion factor  $\alpha_{\text{HCN}}$ , that  $\alpha_{\text{HCN}}$  is  $\sim 3$  times lower in (U)LIRGs. To test the effect of this varying  $\alpha_{\text{HCN}}$  on the dense gas SF law, we applied a value of  $1/2\alpha_{\text{HCN}}^{\text{MW}}$  to LIRGs ( $10^{11}L_{\odot} \leq L_{\text{FIR}} \leq 10^{12}L_{\odot}$ ) and a value of  $1/3\alpha_{\text{HCN}}^{\text{MW}}$  to (U)LIRGs ( $L_{\text{FIR}} \geq 10^{12}L_{\odot}$ ). In this case, we found the power-index of  $\Sigma_{\text{SFR}}-\Sigma_{\text{dense}}$  relation is only slightly changed from  $1.01 \pm 0.02$  to  $1.09 \pm 0.02$ . The slopes fitted for normal galaxies and (U)LIRGs separately are  $0.98 \pm 0.05$  and  $0.97 \pm 0.03$ , respectively, agreeing well with each other within errors.

We notice that García-Burillo et al. (2012) utilized sizes of the star forming regions determined from optical/NIR images of hydrogen recombination lines ( $H_{\alpha}$  and  $P_{\alpha\alpha}$ ), which suffer from heavy dust extinction especially in the dense H II regions in starbursts. We find that the  $H_{\alpha}/P_{\alpha\alpha}$  sizes of García-Burillo et al. (2012) are roughly  $2 - 4\times$  smaller than our RC sizes for the same luminous infrared galaxies. We suspect that this could be the main reason to cause the discrepancy between their results with ours. Besides, the (U)LIRGs sample of García-Burillo et al. (2012) includes also high- $z$  galaxies (mostly QSOs), whose IR luminosities are likely to be contaminated by AGNs. This could be another reason for the steeper slope of (U)LIRGs found in their work. Another factor that might affect  $\Sigma_{\text{SFR}}/\Sigma_{\text{dense}}$  is the FIR 60-to-100  $\mu\text{m}$  color [ $C(60/100)$ ]. GS04b found a weak correlation between  $L_{\text{IR}}/L_{\text{HCN}}$  and the FIR color, which indicated that the warm dust temperature  $T_{\text{dust}}$  also plays a role in the ratio of SFRs-to-dense gas. More details related to FIR 60-to-100  $\mu\text{m}$  color are given in the Appendix C.

### 5.4. Toward a better understanding of SF law

Recent studies of spatially resolved SF laws in nearby star forming galaxies at scales of  $\sim 1$  kpc or less found linear  $\Sigma_{\text{SFR}}-\Sigma_{\text{H}_2}$  relations with typical scatter in the range  $0.2 - 0.3$  dex (Kennicutt et al. 2007; Blanc et al. 2009; Rahman et al. 2011; Verley et al. 2010; Bigiel et al. 2008, 2011; Schruba et al. 2011; Rahman et al. 2012). This includes azimuthally-averaged studies (Wong & Blitz 2002; Murgia et al. 2002; Schuster et al. 2007) and pixel-by-pixel analyses (Kennicutt et al. 2007; Bigiel et al. 2008, 2011; Leroy et al. 2008, 2013; Schruba et al. 2012).

Although this study examines globally-averaged properties, our sample spans a larger range ( $\sim 10^6$ ) in densities of both SFR and molecular gas than previous resolved studies ( $\sim 10^{2-4}$ ). We found an approximately linear  $\Sigma_{\text{SFR}}-\Sigma_{\text{H}_2}$  relation as well (using constant  $\alpha_{\text{CO}}$ ). However, we found much larger scatter in our derived global  $\Sigma_{\text{SFR}}-\Sigma_{\text{H}_2}$  relations (with scatter  $\sim 0.40$  dex), especially toward low luminosity end where atomic gas H I, rather than H<sub>2</sub>, is dominated in the disks of galaxies (with scatter  $\sim 0.55$  dex, see Fig. 3 & 4). This discrepancy implies that the scatter in the observed relations between  $\Sigma_{\text{SFR}}$  and  $\Sigma_{\text{H}_2}$  is mainly driven by galaxy-to-galaxy variations, particularly reflected in low-luminosity galaxies which have low-metallicity and are dominated by atomic gas. Indeed, Schruba et al. (2011), which studied the spatially resolved  $\Sigma_{\text{SFR}}-\Sigma_{\text{H}_2}$  relation in the atomic gas dominated regime in nearby galaxies using stacking technique, found a much larger scatter in  $\Sigma_{\text{SFR}}-\Sigma_{\text{H}_2}$  relation compared with previous studies on molecular gas rich regions. But once the galaxy-to-galaxy scatter was removed, they found a remarkably tight, linear  $\Sigma_{\text{SFR}}-\Sigma_{\text{H}_2}$  relation (with scatter around  $\sim 0.25$  dex).

It is interesting to discuss why the global  $\Sigma_{\text{SFR}}-\Sigma_{\text{H}_2}$  relation exhibits much larger scatter than the resolved relations. The dispersion of  $\alpha_{\text{CO}}$  values among different type of galaxies seems to be usually larger than that within a single galaxy. A generally flat profile of  $\alpha_{\text{CO}}$  as a function of galactocentric radius was observed (except that the central  $\alpha_{\text{CO}}$  value with  $\sim 1$  kpc can be a few of factors below) (Sandstrom et al. 2013; Narayanan et al. 2012). Secondly, some part of the global scatter could be physically real, possibly reflecting the unknown plane thickness variation, different stellar mass, dust abundances, metallicity and SF histories from galaxy to galaxy, or any further parameters that are important in setting the global SFRs. Another important reason could be that the global molecular gas measurements contain diffuse molecular gas - meaning unbound material and the low density outskirts of bound clouds - that extend over whole disks ( $\sim$  kpc) which however could be easily resolved out by the studies at sub-kpc scale as they often adopted high-resolution interferometry measurements. Since this global diffuse molecular gas is not directly associated with SF activity, we thus see a weaker  $\Sigma_{\text{SFR}}-\Sigma_{\text{H}_2}$  correlation in our global studies.

Several studies in literature have derived a variety of power-law indices for the  $\Sigma_{\text{SFR}}-\Sigma_{\text{H}_2}$  relation, ranging from  $N < 1$  (e.g., Blanc et al. 2009),  $N \sim 1$  (e.g., Wong & Blitz 2002; Bigiel et al. 2008),  $N \sim 1.3 - 1.5$  (K98; Kennicutt et al. 2007; Schruba et al. 2010) to  $N \sim 1.7 - 2.0$  (Bouché et al. 2007; Verley et al. 2010). A contributing factor to the wide range of observed power-law indices stems from the different scales over which surface densities have been inferred (i.e., global scales, radial profiles, and pixel-by-pixel). Within the same individual galaxy, the resolved  $\Sigma_{\text{SFR}}-\Sigma_{\text{H}_2}$  relation may depend on the averaging aperture size on small scales ( $\leq 300$  pc) (Schruba et al. 2010; Verley et al. 2010; Calzetti et al. 2012). Another contributing factor is the differences in estimators of SFR and SF size adopted across various studies since they directly affect the densities and thus the derived SF laws. Finally, our work clearly shows that the  $\Sigma_{\text{SFR}}-\Sigma_{\text{H}_2}$  relation is sensitive to the application of  $\alpha_{\text{CO}}$ .

Furthermore, the choice and weighting of sample data also plays a significant role in the resulting power indices of SF laws. Previous studies on sub-kpc scale demonstrated that the  $\Sigma_{\text{SFR}} - \Sigma_{\text{H}_2}$  relation is roughly linear in the regime  $10 < \Sigma_{\text{H}_2} < 100 M_{\odot} \text{ pc}^{-2}$  where normal spiral galaxies are found, and gets super-linear in the regime  $\Sigma_{\text{H}_2} > 100 M_{\odot} \text{ pc}^{-2}$  of starburst galaxies (e.g., Bigiel et al. 2008; Leroy et al. 2013). Our studies on global scales found a similar trend using, for the first time, RC observations. In fact, we find that the slopes of  $\Sigma_{\text{SFR}} - \Sigma_{\text{H}_2}$  relation change from  $\sim 1.0$  to  $\sim 1.2$  when more and more (U)LIRGs are included (when a uniform  $\alpha_{\text{CO}}$  was used). That is the larger weight to the (U)LIRGs sample or the data with  $\Sigma_{\text{H}_2} > 100 M_{\odot} \text{ pc}^{-2}$ , the steeper slopes in SF laws related to molecular gas and total gas. This may imply a density-dependent SF efficiency of gas, i.e., the higher density exhibits higher SF efficiency. A similar trend was also pointed out by GS04b, which studied the global IR-CO luminosity correlation of local (U)LIRGs. The studies of high- $z$  galaxies indicate a similar behavior as well (Bouché et al. 2007; Daddi et al. 2010; Bothwell et al. 2010).

Our work showed that the linear  $\Sigma_{\text{SFR}} - \Sigma_{\text{dense}}$  relation is independent of the galaxy sample and IR luminosity, so that the dense SF law can be described by a universal one-function law across all galaxy types. Not only at global scales does the SFR density exhibit a tight and linear correlation with the dense gas density as showed in our work, the HCN surveys of Galactic dense cores and dense clumps even extend the linear luminosity correlation down to GMC scales (Wu et al. 2005, 2010). As we adopted lower  $\alpha_{\text{HCN}}$  for (U)LIRGs ( $1/3 - 1/2\alpha_{\text{MW}}^{\text{HCN}}$ ), the slope is only slightly changed and still close to unity. The luminosities of other dense gas tracer such as HNC(1-0), HCO<sup>+</sup>, CN(2-1) and CS(3-2) were observed to vary linearly with  $L_{\text{FIR}}$  as well (Baan et al. 2008; Zhang et al. 2014).

## 6. SUMMARY

We have examined the relations between the galaxy-averaged surface densities of the various gas components (atomic, molecular, total gas and dense molecular gas) and SFR in a sample of 181 local galaxies with IR luminosities spanning  $\sim 5$  orders of magnitude ( $10^{7.8} - 10^{12.3} L_{\odot}$ ). We have taken a novel approach and used high-resolution radio continuum observations to accurately measure the sizes of the areas of active star formation within the galaxies – a key step as it directly affects the inferred gas and SFR surface densities.

We found there is no correlation between  $\Sigma_{\text{SFR}}$  and  $\Sigma_{\text{HI}}$ , and that  $\Sigma_{\text{HI}}$  does not exceed a maximum value of  $\sim 25 M_{\odot} \text{ pc}^{-2}$ . We have explored the  $\Sigma_{\text{SFR}} - \Sigma_{\text{H}_2}$  relation for different values of the  $\alpha_{\text{CO}}$  factor. Adopting a Galactic  $\alpha_{\text{CO}}$  to all galaxies, a roughly linear power-law index ( $N = 1.14 \pm 0.02$ ) was found. If a more realistic  $\alpha_{\text{CO}}$ -value [ $0.8 M_{\odot} (\text{K km s}^{-1} \text{ pc}^2)^{-1}$ ] is applied to the (U)LIRGs in our sample the result is a bimodal SF law, i.e., two nearly linear  $\Sigma_{\text{SFR}} - \Sigma_{\text{H}_2}$  correlations, indicating that separate SF modes might exist for (U)LIRGs and disk galaxies. A unimodal, but significantly steeper ( $N = 1.62 \pm 0.04$ ),  $\Sigma_{\text{SFR}} - \Sigma_{\text{H}_2}$  relation is recovered if a continuously-varying  $\alpha_{\text{CO}}$  conversion factor is applied. The global  $\Sigma_{\text{SFR}}$  shows steeper functions of total gas

density  $\Sigma_{\text{gas}}$  than those of  $\Sigma_{\text{H}_2}$  (the slopes depend on the  $\alpha_{\text{CO}}$  as well), and are tighter than  $\Sigma_{\text{SFR}} - \Sigma_{\text{H}_2}$  relation among low-luminosity galaxies. The dense molecular gas density  $\Sigma_{\text{dense}}$  shows the best correlation with  $\Sigma_{\text{SFR}}$ , which is exactly linear with index  $N = 1.01 \pm 0.02$ . Fitting the normal galaxies and (U)LIRGs separately yields the same linear slopes.

Out of these results the following picture emerges. The SF is more directly related to molecular gas than atomic gas. But the seeming roughly linear relation of  $\Sigma_{\text{SFR}} - \Sigma_{\text{H}_2}$  can easily get super-linear as a varying- $\alpha_{\text{CO}}$  was adopted and the number of (U)LIRGs increases. The fact that the low-luminosity galaxies lie significantly above the  $\Sigma_{\text{SFR}} - \Sigma_{\text{H}_2}$  relation derived for whole sample suggest there could be some other parameter apart from the molecular gas content that determines the SF in these galaxies. Unlike the molecular SF law, the linear  $\Sigma_{\text{SFR}} - \Sigma_{\text{dense}}$  relation is independent of the choice of sample (thus galaxy luminosity) and the adopted  $\alpha_{\text{HCN}}$  factor, suggesting the basic units of SF in galaxies are in dense cores.

This work is partially supported by NSFC grant Nos. 11173059 and 11390373, and CAS No. XDB09000000. This research has made use of the NASA IPAC Extragalactic Database (NED) which is operated by the Jet Propulsion Laboratory, California Institute of Technology, under contract with the National Aeronautics and Space Administration.

TABLE 1  
LUMINOSITIES

Name	D	$L_{CO}$	$L_{HCN}$	$L_{IR}$	$L_{RC}$	Ref.	Name	D	$L_{CO}$	$L_{HCN}$	$L_{IR}$	$L_{RC}$	Ref.
<b>Normal Galaxies</b>													
NGC 0134	21.38	3.76	0.4	10.62	3.48	13, 21, 36, 44	NGC 0174	49.74	12.81	1.8	10.93	3.58	13, 21, 36, 50
NGC 0253	4.11	15.26	0.66	10.69	5.13	2, 20, 36, 43	NGC 0520	30.59	28.84	0.62	10.92	13.31	3, 29, 36, 42
NGC 0598	0.81	0.06	...	9.04	-6.14	3, 36, 42	NGC 0628	10.55	6.99	...	9.99	-4	6, 36, 42
NGC 0660	12	10	0.17	10.47	0.35	3, 20, 36, 42	NGC 0772	34.52	46.93	...	10.61	3.85	3, 36, 42
NGC 0891	9.17	7.68	0.22	10.33	0.65	1, 20, 36, 48	NGC 0925	9.1	1.94	...	9.39	-5.94	3, 36, 48
NGC 0931	67.26	0.66	1.85	10.85	0.8	14, 24, 40, 44	NGC 1022	19.48	3.13	0.15	10.35	-4.18	1, 20, 36, 44
NGC 1055	13.63	10.09	0.24	10.25	-1.83	1, 20, 36, 42	NGC 1058	8.8	0.3	...	8.93	-6.31	8, 37, 42
NGC 1097	16.87	4.68	...	10.71	7.73	9, 36, 46	NGC 1266	29.7	13.64	0.52	10.48	5.53	16, 34, 36, 52
NGC 1530	37.01	16.08	0.53	10.71	4.63	3, 29, 36, 42	NGC 1569	4.11	0.02	...	9.39	-5.67	3, 36, 42
NGC 1667	61.83	16.64	6.83	10.97	28.27	14, 24, 36, 44	NGC 1808	12.56	6.63	0.7	10.71	3.4	11, 21, 36, 46
NGC 2273	28.54	0.76	0.21	10.25	-1.04	14, 24, 36, 49	NGC 2276	36.96	9.78	0.38	10.83	41.47	1, 20, 36, 42
NGC 2403	4.11	0.22	...	9.4	-5.96	3, 36, 42	NGC 2764	41.36	6.17	0.1	10.33	-3.76	16, 34, 41, 52
NGC 2841	13.42	8.24	...	9.72	-4.62	3, 38, 42	NGC 2903	8.53	5.16	0.15	10.22	-2.54	6, 20, 36, 42
NGC 2976	4.11	0.25	...	8.92	-6.3	3, 36, 42	NGC 3031	4.11	0.47	...	9.57	-5.63	9, 36, 42
NGC 3032	25.22	1.45	0.04	9.67	-5.9	15, 32, 41, 52	NGC 3079	19.51	29.68	1.22	10.79	30.98	1, 20, 36, 43
NGC 3147	43.05	61.65	0.64	10.93	15.78	3, 29, 36, 42	NGC 3310	17.06	1	...	10.47	0.74	3, 36, 42
NGC 3338	19.12	1.7	...	9.67	-5.12	3, 37, 42	NGC 3351	8.71	2.8	...	9.71	-6.01	2, 36, 42
NGC 3368	10.42	1.62	...	9.54	-5.98	3, 36, 42	NGC 3486	8.41	0.83	...	9.22	-5.94	3, 36, 42
NGC 3504	26.36	10.89	0.64	10.69	16.38	2, 25, 36, 42	NGC 3521	8.28	13.27	...	10.12	-3.47	2, 36, 42
NGC 3556	12.09	3.69	0.1	10.24	-1.44	1, 20, 36, 42	NGC 3620	19.18	5.15	0.66	10.67	0.16	13, 21, 36, 51
NGC 3627	7.34	5.9	0.05	10.1	-3.48	1, 20, 36, 42	NGC 3628	8.67	8	0.28	10.12	-2.17	1, 20, 36, 43
NGC 3631	20.22	10.99	...	10.23	-2.29	2, 36, 42	NGC 3665	34.83	2.56	0.12	9.97	4.34	16, 34, 41, 52
NGC 3675	11.72	4.84	...	9.85	-5.64	3, 36, 42	NGC 3726	14.02	3.46	...	9.75	-5.51	3, 36, 42
NGC 3893	16.38	4.11	0.29	10.2	-1.94	1, 20, 36, 42	NGC 3938	12.4	3.47	...	9.78	-5.23	10, 36, 42
NGC 4030	20.14	18.65	0.66	10.47	1.07	1, 20, 36, 42	NGC 4038	21.1	12.52	0.16	10.82	7.31	3, 21, 36, 44
NGC 4041	21.57	8.31	0.23	10.38	-0.67	3, 20, 36, 42	NGC 4150	4.11	0.01	...	7.85	-6.4	15, 32, 41, 52
NGC 4178	19.36	0.55	...	9.53	-5.04	3, 37, 42	NGC 4189	20.06	2.46	...	9.71	-5.54	3, 37, 42
NGC 4254	16.3	18.39	...	10.59	6.96	4, 36, 42	NGC 4258	6.85	3.08	...	9.67	-3.64	10, 39, 42
NGC 4294	19.19	0.36	...	9.59	-5.47	3, 37, 42	NGC 4299	15.9	0.25	...	9.4	-5.88	3, 37, 42
NGC 4303	19.8	18.41	...	10.73	14.43	4, 36, 42	NGC 4321	19.47	22.16	...	10.6	5.51	4, 36, 42
NGC 4394	19.08	2.49	...	9.28	-6.37	3, 37, 46	NGC 4402	18.6	4.4	...	9.94	-5.29	4, 36, 42
NGC 4414	8.48	5.19	0.11	9.91	-4.34	2, 20, 36, 42	NGC 4459	19.53	0.52	0.06	9.48	-6.32	15, 32, 40, 52
NGC 4501	19.41	19.63	...	10.53	6.09	4, 36, 42	NGC 4519	19.67	1.14	...	9.71	-5.58	3, 37, 42
NGC 4526	18.79	1.55	0.12	9.88	-5.93	15, 32, 36, 50	NGC 4535	19.75	13.83	...	10.26	-2.78	4, 36, 42
NGC 4548	18.79	6.13	...	9.49	-6.21	4, 37, 42	NGC 4561	19.42	1.11	...	9.2	-6.08	3, 37, 42
NGC 4569	18.8	16.25	0.23	10.2	-2.87	2, 22, 36, 42	NGC 4571	19.43	3.51	...	9.38	-6.15	3, 37, 49
NGC 4579	19.32	8.13	...	10.07	-2.08	2, 36, 42	NGC 4631	7.35	2.17	0.06	10.18	1.36	7, 20, 36, 43
NGC 4639	18.97	3.33	...	9.38	-6.08	9, 37, 42	NGC 4647	19.1	5.53	...	10	-4.03	4, 36, 42
NGC 4651	19.12	3.13	...	9.91	-4.94	3, 36, 42	NGC 4654	19.55	6.64	...	10.31	-0.78	4, 36, 42
NGC 4689	19.79	7.58	...	9.47	-5.81	2, 37, 42	NGC 4698	19.51	0.84	...	9.07	-6.34	3, 37, 46
NGC 4710	19.23	2.2	0.11	9.88	-5.74	16, 34, 36, 52	NGC 4713	19.43	0.65	...	9.73	-4.4	3, 37, 42
NGC 4736	4.37	1.3	...	9.64	-5.79	2, 36, 42	NGC 4826	16.3	14.12	0.44	10.52	-3.11	1, 20, 36, 42
NGC 4945	5.2	15.74	0.47	10.73	7.19	9, 31, 36, 43	NGC 5005	14.1	12.36	0.62	10.24	-1.89	1, 20, 36, 42
NGC 5033	12.63	6.19	0.17	10.06	-3	9, 24, 36, 42	NGC 5055	7.44	6.35	0.11	10.03	-4.08	1, 20, 36, 42
NGC 5194	7.53	14	0.06	10.29	3.71	10, 22, 36, 42	NGC 5236	4.7	7.07	0.06	10.33	0.06	1, 28, 36, 46
NGC 5347	32.18	0.39	0.16	9.95	-5.6	14, 24, 41, 44	NGC 5457	4.94	5.31	...	9.93	-4.21	2, 36, 42
NGC 5678	32.23	20.62	0.99	10.61	7.27	1, 20, 36, 42	NGC 5713	30.26	11.33	0.38	10.82	10.91	1, 20, 36, 42
NGC 5775	27.61	16.2	0.84	10.82	16.49	1, 20, 36, 42	NGC 5861	28.5	4.13	0.12	10.49	-3.24	13, 21, 36, 44
NGC 5936	55.4	12.38	0.6	10.97	11.78	17, 35, 36, 50	NGC 6014	34.34	1.87	0.05	9.71	-5.82	16, 34, 41, 48
NGC 6207	17.55	0.75	...	9.68	-5.11	3, 37, 42	NGC 6217	24.26	6.46	...	10.37	-0.77	2, 36, 42
NGC 6503	6.27	0.99	...	9.22	-6.23	3, 36, 42	NGC 6643	25.79	8.78	...	10.51	1.14	6, 36, 42
NGC 6814	21.5	1.8	0.18	10.15	-3.65	14, 24, 36, 44	NGC 6946	4.16	5.16	0.23	9.94	-3.5	2, 20, 36, 42
NGC 6951	23.01	18.86	0.34	10.53	-2.09	2, 22, 36, 44	NGC 7252	64.9	9.27	...	10.73	6.4	3, 37, 48
NGC 7331	14.38	27.11	0.37	10.56	1.74	6, 20, 36, 42	NGC 7465	27.90	2.46	0.02	10.11	-4.62	16, 34, 36, 48
NGC 7479	33.56	23.08	0.94	10.82	8.02	9, 20, 36, 42	NGC 7582	21.66	7.98	0.41	10.88	8.76	13, 21, 36, 46
UGC 4013	122.84	4.38	2.31	10.78	4.07	14, 24, 41, 44	He 2-10	12	2.1	0.04	10.04	-4.96	19, 33, 40, 44
IC 342	4.32	16.32	0.4	10.11	-1.38	2, 20, 36, 42	IC 676	21	1.09	0.02	9.69	-5.85	16, 34, 41, 48
Maffei 2	4.1	6.72	0.09	9.73	-5.82	2, 30, 40, 44							
<b>(U)LIRGs</b>													
Arp 055	165.58	121.58	4.31	11.68	114.32	1, 20, 36, 42	Arp 148	147.13	45.54	4.84	11.6	56.54	1, 20, 36, 42
Arp 193	101.84	48.55	2.83	11.66	122.66	5, 23, 36, 42	Arp 220	80.89	90.59	10.78	12.2	248.83	3, 29, 36, 42
IC 0883	101.84	55.81	...	11.66	122.66	3, 36, 42	IC 1623	80.72	118.73	7.36	11.65	158.1	1, 20, 36, 44
IC 5179	44.65	21.78	3.06	11.11	32.96	1, 20, 36, 45	III Zw 35	110	18.55	2.7	11.57	52.53	17, 35, 36, 48
00335-2732	281.69	52.01	50.59	11.94	100.89	13, 21, 41, 44	00506+7248	65.2	22.81	0.78	11.44	56.67	17, 35, 36, 48
01364-1042	205.92	48.23	12.11	11.83	79.85	13, 21, 36, 50	03056+2034	114.09	30.09	1.02	11.25	20.23	13, 21, 40, 44
05189-2524	173.26	67.85	6.59	12.1	98.12	1, 20, 36, 44	05414+5840	61.63	38.19	2.34	11.22	39.96	13, 21, 36, 44
07329+1149	69.15	9.9	0.51	11.08	20.49	17, 35, 36, 48	08071+0509	222.9	86.16	7.82	11.84	160.05	13, 21, 41, 49
10039-3338	143.7	32.83	7.69	11.71	51.42	18, 21, 36, 44	10173+0828	204.09	54.36	3.78	11.78	47.43	5, 35, 36, 44
10565+2448	173.3	56.93	10.69	11.97	201.3	1, 20, 36, 48	11506-3851	40.26	8.93	2.7	11.15	12.22	13, 21, 36, 49
12112+0305	313.55	114.95	14.65	12.29	283.45	13, 27, 36, 52	13126+2452	54.08	16.9	0.34	11.09	4.27	13, 21, 36, 50
16399-0937	113.18	37	1.43	11.52	77.44	13, 21, 36, 44	17138-1017	75.0	22.62	0.67	11.39	40.24	17, 35, 41, 48

TABLE 1 — Continued

Name	D	$L_{\text{CO}}$	$L_{\text{HCN}}$	$L_{\text{IR}}$	$L_{\text{RC}}$	Ref.	Name	D	$L_{\text{CO}}$	$L_{\text{HCN}}$	$L_{\text{IR}}$	$L_{\text{RC}}$	Ref.
17208-0014	175.81	115.15	16.38	12.35	348.64	5, 21, 36, 47	17526+3253	103.36	27.18	1.59	11.08	21.72	13, 21, 41, 49
18090+0130	121.3	41.23	1.55	11.56	96.41	17, 35, 36, 48	18293-3413	79.89	92.39	4.94	11.81	166.95	1, 20, 36, 48
20550+1656	147.84	42.93	2.53	11.87	106.58	13, 21, 36, 44	22025+4205	60.68	8.09	2.07	10.97	8.93	13, 21, 36, 44
23365+3604	258.74	83.84	16.35	12.11	224.29	1, 20, 36, 48	Mrk 0231	173.37	62.08	20.78	12.48	863.92	5, 27, 36, 42
Mrk 0266	121.77	76.16	1.29	11.83	192.31	3, 26, 37, 52	Mrk 0273	159.66	66.72	14.35	12.14	434.95	1, 27, 36, 42
Mrk 0331	71.92	42.55	2.76	11.41	37.36	1, 20, 36, 44	Mrk 1027	121.3	48.95	2.68	11.38	87.26	1, 20, 36, 42
NGC 0023	62.4	16.23	0.65	11.08	23.88	17, 35, 36, 50	NGC 0034	80.92	35.32	8.97	11.46	39.59	14, 24, 36, 50
NGC 0695	130.6	89.49	4.73	11.63	146.25	1, 20, 36, 42	NGC 0828	72.73	78.92	0.81	11.32	59.42	3, 29, 36, 42
NGC 1068	15.46	29.56	2.99	11.37	132.3	9, 20, 36, 42	NGC 1144	115.93	71.3	1.95	11.39	242.85	1, 20, 37, 42
NGC 1365	21.84	43.28	3.55	11.17	15.11	1, 20, 36, 44	NGC 1614	64.78	32.86	1.25	11.61	62.99	12, 20, 36, 44
NGC 2146	15.34	14.34	1.03	11	23.85	1, 20, 36, 44	NGC 2369	44.72	27.09	1.97	11.1	28.54	13, 21, 36, 51
NGC 2388	60.4	22.85	1.14	11.25	21.8	17, 35, 36, 52	NGC 2623	76.71	24.47	1.41	11.52	60.98	3, 26, 36, 42
NGC 3034	4.89	10.34	0.45	11.03	15.51	1, 20, 36, 42	NGC 3110	73.24	24.74	1.02	11.29	76.4	17, 35, 36, 48
NGC 3256	35.86	46.43	2.48	11.56	95	11, 21, 36, 46	NGC 3690	48.02	34.41	2.62	11.88	175.15	3, 29, 36, 47
NGC 5135	54.08	30.5	2.57	11.19	61.49	1, 20, 36, 45	NGC 5653	55.31	16.44	0.63	11.05	20.39	17, 35, 36, 48
NGC 6240	106.71	83.26	14.71	11.85	527.69	5, 21, 36, 45	NGC 6701	59.07	32.51	1.3	11.07	30.72	1, 20, 36, 42
NGC 6921	59.41	30.22	2.41	11.07	5.17	3, 20, 40, 42	NGC 7130	68.58	44.06	3.21	11.37	96.58	1, 20, 36, 45
NGC 7469	68.08	33.31	2.01	11.61	93.98	1, 20, 36, 42	NGC 7552	22.05	11	0.69	11.05	9.66	11, 21, 36, 45
NGC 7591	67.37	16.45	0.57	11.01	15.87	17, 35, 41, 50	NGC 7771	58.04	30.46	3.99	11.34	50.43	12, 23, 36, 42
UGC 1845	63.96	19.79	1.09	11.08	24.14	17, 35, 36, 48	UGC 5101	164.93	48.77	11.71	11.95	546.91	1, 20, 36, 42
VII Zw 31	220.72	226.41	10.69	11.92	237.84	3, 20, 36, 44	ZW 049.057	53.38	8.48	1.53	11.18	10.99	5, 21, 36, 47

REFERENCES. — **CO data:** [1] Gao & Solomon (2004a); [2] Kuno et al. (2007); [3] Young et al. (1995); [4] Chung et al. (2009b); [5] Papadopoulos et al. (2010); [6] Nishiyama & Nakai (2001); [7] Paglione et al. (2001); [8] Sage (1993); [9] Maiolino et al. (1997); [10] Helfer et al. (2003); [11] Smith & Harvey (1996); [12] Elfhag et al. (1996); [13] Baan et al. (2008); [14] Curran et al. (2000); [15] Young et al. (2008); [16] Crocker et al. (2012); [17] García-Burillo et al. (2012); [18] Gao & Solomon (1999); [19] Bayet et al. (2009). **HCN data:** [20] Gao & Solomon (2004a); [21] Baan et al. (2008); [22] Krips et al. (2008); [23] Juneau et al. (2009); [24] Curran et al. (2000); [25] Matsushita et al. (2010); [26] Imanishi et al. (2009); [27] Graciá-Carpio et al. (2008); [28] Huettemeister et al. (1995); [29] Solomon et al. (1992); [30] Nguyen et al. (1992); [31] Wang et al. (2004); [32] Krips et al. (2010); [33] Imanishi et al. (2007); [34] Crocker et al. (2012); [35] García-Burillo et al. (2012). **IR data:** [36] Sanders et al. (2003); [37] Moshir et al. (1990); [38] Lisenfeld et al. (2007); [39] Rice et al. (1988); [40] Joint Iras Science (1994); [41] Moshir et al. (1993). **1.4 GHz RC data:** [42] Condon et al. (2002); [43] Strickland et al. (2004); [44] Condon et al. (1998); [45] Condon et al. (1996); [46] Condon (1987); [47] Baan & Klöckner (2006); [48] Yun et al. (2001); [49] measured from our radio maps; [50] Condon et al. (1990); [51] Mauch et al. (2008); [52] Becker et al. (2003).

NOTE. — D is the distance in [Mpc];  $L_{\text{CO}}$  and  $L_{\text{HCN}}$  are line luminosities in [ $10^8 \text{ K km}^{-1} \text{ pc}^2$ ];  $L_{\text{IR}}$  is the log of total IR luminosity ( $8 - 1000 \mu\text{m}$ ) in [ $L_{\odot}$ ]; and  $L_{\text{RC}}$  is the luminosity of 1.4 GHz RC in [ $10^{21} \text{ W Hz}^{-1}$ ].

TABLE 2  
SURFACE DENSITY

Name	Diameter	$\log \Sigma_{\text{HI}}$	$\log^a \Sigma_{\text{H2}}$	$\log^b \Sigma_{\text{H2}}$	$\log^a \Sigma_{\text{gas}}$	$\log \Sigma_{\text{den}}$	$\log \Sigma_{\text{IR}}$	$\log \Sigma_{\text{RC}}$	Ref.
	[arcsec]			$[\text{M}_{\odot} \text{pc}^{-2}]$			$[\text{M}_{\odot} \text{yr}^{-1} \text{kpc}^{-2}]$		
<b>Normal Galaxies</b>									
NGC 0134	150	0.29	0.66	0.93	0.81	0.02	-1.83	-1.84	4, 33
NGC 0174	5.1	...	3.39	3.02	3.39	2.88	0.67	0.37	AU23,
NGC 0253	96	0.82	3.09	2.81	3.09	2.06	0.05	0.04	1, 24
NGC 0520	4.5	0.73	4.28	3.62	4.28	2.94	1.19	1.19	AC205, 27
NGC 0598	1713	0.89	-0.39	-0.12	0.91	...	-2.45	-2.34	2, 18
NGC 0628	329	0.62	0.86	1.13	1.06	...	-2.47	-2.41	1, 13
NGC 0660	18	0.19	3.43	3.04	3.43	1.99	0.37	0.34	AL296, 17
NGC 0772	79	0.48	1.9	2	1.92	...	-1.7	-1.69	1, 19
NGC 0891	238	0.21	1.3	1.57	1.33	0.1	-1.76	-1.65	4, 17
NGC 0925	186	0.85	0.93	1.2	1.19	...	-2.35	-2.33	1, 13
NGC 0931	50	...	-0.14	0.13	-0.14	0.65	-1.66	-2.02	9,
NGC 1022	5.0	0.4	3.61	3.17	3.61	2.62	0.96	0.67	AG278+AL377, 20
NGC 1055	90	0.72	1.92	2.02	1.95	0.64	-1.33	-1.3	1, 17
NGC 1058	90	0.5	0.78	1.05	0.96	...	-2.04	-2.21	AP404, 15
NGC 1097	28	0.14	2.42	2.36	2.42	...	-0.08	-0.02	AB775, 28
NGC 1266	5.1	...	3.87	3.34	3.87	2.78	0.69	0.89	11,
NGC 1530	31	0.77	2.18	2.2	2.2	1.04	-0.85	-0.9	4, 15
NGC 1569	74	1.26	0.52	0.79	1.33	...	-0.86	-0.68	1, 16
NGC 1667	33	...	1.7	1.87	1.7	1.65	-1.11	-0.9	AA281,
NGC 1808	17	0.72	3.26	2.93	3.26	2.62	0.61	0.51	AD231, 29
NGC 2273	1.7	0.3	3.6	3.16	3.6	3.38	1.47	1.55	AY044, 31
NGC 2276	76	1.02	1.19	1.46	1.41	0.12	-1.51	-1.04	1, 15
NGC 2403	328	0.85	0.18	0.45	0.93	...	-2.15	-2.15	1, 13
NGC 2764	9.4	0.93	2.71	2.55	2.72	1.25	-0.26	-0.48	11, 20
NGC 2841	216	0.44	1.09	1.36	1.18	...	-2.55	-2.35	1, 13
NGC 2903	122	0.74	1.77	1.92	1.81	0.56	-1.22	-1.21	1, 13
NGC 2976	154	0.9	0.89	1.16	1.2	...	-1.85	-1.97	1, 13
NGC 3031	466	0.35	0.2	0.47	0.58	...	-2.31	-2.27	1, 18
NGC 3032	15	-0.16	2.1	2.14	2.1	0.9	-0.81	-1	12, 38
NGC 3079	38	0.44	2.83	2.64	2.83	1.78	-0.4	0.01	ASTUD, 30
NGC 3147	60	0.28	2.06	2.11	2.07	0.42	-1.35	-1.3	1, 15
NGC 3310	32	0.97	1.62	1.81	1.71	...	-0.43	-0.45	AD176, 15
NGC 3338	145	0.59	0.44	0.71	0.82	...	-2.55	-2.42	1, 19
NGC 3351	16	0.28	3.25	2.93	3.25	...	0.08	-0.22	AO73, 13
NGC 3368	97	0.58	1.3	1.57	1.38	...	-1.78	-1.91	1, 18
NGC 3486	129	0.91	0.94	1.21	1.23	...	-2.09	-1.94	1, 18
NGC 3504	8.0	0.43	3.48	3.08	3.48	2.59	0.6	0.88	AS204, 31
NGC 3521	166	1.03	1.94	2.03	1.99	...	-1.55	-1.54	1, 13
NGC 3556	185	1.12	0.96	1.23	1.35	-0.26	-1.86	-1.8	1, 15
NGC 3620	26	...	2.41	2.35	2.41	1.86	-0.16	-0.4	10,
NGC 3627	160	0.73	1.73	1.89	1.77	-0.03	-1.43	-1.41	1, 13
NGC 3628	71	0.85	2.42	2.36	2.43	1.3	-0.85	-0.73	1, 21
NGC 3631	85	...	1.67	1.85	1.67	...	-1.64	-1.63	1,
NGC 3665	31	...	1.44	1.69	1.44	0.46	-1.48	-0.86	11,
NGC 3675	89	0.56	1.74	1.9	1.77	...	-1.55	-1.74	1, 18
NGC 3726	174	0.8	0.86	1.13	1.13	...	-2.37	-2.43	1, 15
NGC 3893	81	1.19	1.46	1.71	1.65	0.65	-1.45	-1.38	1, 15
NGC 3938	149	0.82	1.1	1.37	1.28	...	-2.1	-2.1	1, 18
NGC 4030	74	0.55	2.02	2.09	2.03	0.91	-1.31	-1.3	1, 22
NGC 4038	49	...	2.16	2.18	2.16	0.6	-0.66	-0.72	9,
NGC 4041	35	...	2.26	2.25	2.26	1.03	-0.8	-0.81	AC101,
NGC 4150	17	-0.31	1.74	1.9	1.74	0.59	-0.65	-1.21	11, 15
NGC 4178	166	0.93	-0.18	0.09	0.96	...	-2.8	-2.53	1, 18
NGC 4189	73	0.88	1.16	1.43	1.34	...	-1.96	-2	9, 14
NGC 4254	137	0.96	1.66	1.84	1.74	...	-1.54	-1.4	1, 14
NGC 4258	207	0.57	1.28	1.55	1.36	...	-1.97	-1.59	BG062, 18
NGC 4294	56	1.3	0.59	0.86	1.38	...	-1.8	-1.7	AV298, 14
NGC 4299	45	1.29	0.78	1.05	1.41	...	-1.6	-1.54	AV298, 14
NGC 4303	136	0.84	1.5	1.73	1.59	...	-1.57	-1.37	1, 18
NGC 4321	123	0.51	1.68	1.86	1.71	...	-1.6	-1.51	1, 14
NGC 4394	75	-0.6	1.18	1.45	1.19	...	-2.3	-3.11	1, 14
NGC 4402	54	0.87	1.74	1.89	1.79	...	-1.43	-1.58	5, 14
NGC 4414	71	0.51	2.25	2.24	2.26	0.93	-1.02	-0.94	1, 19
NGC 4459	6.5	...	2.61	2.48	2.61	2.02	-0.03	-0.65	12,
NGC 4501	121	0.6	1.65	1.83	1.69	...	-1.64	-1.47	1, 14
NGC 4519	88	...	0.67	0.94	0.67	...	-2.1	-2.16	1,
NGC 4526	11	0.71	2.66	2.52	2.66	1.87	-0.12	-0.49	5, 39
NGC 4535	133	0.57	1.4	1.66	1.46	...	-1.99	-2.04	1, 14
NGC 4548	96	-0.26	1.37	1.64	1.38	...	-2.32	-2.67	AB342+AC101, 14
NGC 4561	57	1.2	1.05	1.32	1.43	...	-2.14	-2.07	9, 14

TABLE 2 — Continued

Name	Diameter	$\log \Sigma_{\text{HI}}$	$\log^a \Sigma_{\text{H}_2}$	$\log^b \Sigma_{\text{H}_2}$	$\log^a \Sigma_{\text{gas}}$	$\log \Sigma_{\text{den}}$	$\log \Sigma_{\text{IR}}$	$\log \Sigma_{\text{RC}}$	Ref.
	[arcsec]			[ $M_{\odot} \text{ pc}^{-2}$ ]			[ $M_{\odot} \text{ yr}^{-1} \text{ kpc}^{-2}$ ]		
NGC 4569	85	0.61	1.9	2	1.92	0.39	-1.61	-1.62	1, 14
NGC 4571	94	...	1.12	1.39	1.12	...	-2.43	-2.59	1,
NGC 4579	57	0.1	1.92	2.02	1.93	...	-1.4	-1.23	1, 14
NGC 4631	298	0.37	0.75	1.02	0.9	-0.47	-1.9	-1.62	1, 17
NGC 4639	83	0.64	1.22	1.49	1.32	...	-2.3	-2.38	AK205, 18
NGC 4647	74	0.59	1.54	1.76	1.59	...	-1.68	-1.64	9, 18
NGC 4651	54	0.91	1.56	1.78	1.65	...	-1.48	-1.52	1, 14
NGC 4654	108	0.93	1.27	1.54	1.43	...	-1.75	-1.71	1, 14
NGC 4689	68	0.49	1.72	1.88	1.74	...	-2.08	-2.05	1, 14
NGC 4698	81	0.27	0.62	0.89	0.78	...	-2.55	-2.96	AC101+AB342, 14
NGC 4710	11	...	2.79	2.61	2.79	1.81	-0.13	-0.4	5,
NGC 4713	66	1.17	0.69	0.96	1.29	...	-1.83	-1.61	AV298, 14
NGC 4736	104	0.91	1.89	2	1.93	...	-1.01	-1.09	1, 13
NGC 4826	39	0.88	2.64	2.51	2.65	1.47	-0.51	-0.84	AS541, 13
NGC 4945	47	-0.02	3.52	3.1	3.52	2.33	0.51	0.53	10, 26
NGC 5005	69	0.11	2.21	2.22	2.21	1.25	-1.15	-1.11	1, 22
NGC 5033	63	0.79	2.09	2.13	2.11	0.85	-1.13	-1.02	1, 18
NGC 5055	185	0.7	1.62	1.81	1.67	0.18	-1.63	-1.62	1, 13
NGC 5194	284	0.58	1.58	1.79	1.62	-0.44	-1.78	-1.48	1, 13
NGC 5236	321	0.44	1.59	1.79	1.62	-0.13	-1.44	-1.37	1, 13
NGC 5347	36	0.58	0.56	0.83	0.87	0.51	-1.55	-1.81	9, 15
NGC 5457	452	0.58	1.12	1.39	1.23	...	-2.14	-2.06	AC101+AF085, 13
NGC 5678	57	1.02	1.88	1.99	1.94	0.9	-1.36	-1.22	9, 19
NGC 5713	33	0.96	2.15	2.17	2.18	1.01	-0.63	-0.59	AL377, 23
NGC 5775	115	0.62	1.3	1.57	1.38	0.35	-1.63	-1.47	6, 24
NGC 5861	73	...	1.08	1.35	1.08	-0.13	-1.57	-1.88	9,
NGC 5936	9.0	...	2.79	2.61	2.79	1.81	0.12	0.04	5,
NGC 6014	4.4	...	3.01	2.76	3.01	1.76	0.01	-0.15	11,
NGC 6207	76	0.82	0.72	0.99	1.07	...	-1.91	-1.78	9, 19
NGC 6217	16	...	2.73	2.57	2.73	...	-0.23	-0.24	AC205+AC101,
NGC 6503	118	0.68	1.35	1.62	1.43	...	-1.77	-1.93	1, 19
NGC 6643	74	1.08	1.48	1.72	1.63	...	-1.48	-1.51	4, 15
NGC 6814	93	0.73	0.75	1.02	1.04	0.08	-1.85	-1.89	9, 36
NGC 6946	318	0.87	1.56	1.78	1.64	0.56	-1.68	-1.51	1, 13
NGC 6951	82	0.27	1.82	1.95	1.83	0.41	-1.46	-1.7	9, 35
NGC 7252	5.0	...	3.04	2.78	3.04	...	0.26	0.26	AN90,
NGC 7331	146	0.91	1.88	1.99	1.92	0.35	-1.52	-1.56	1, 13
NGC 7465	7.5	0.86	2.84	2.65	2.84	1.11	0.07	-0.07	11, 40
NGC 7479	97.9	0.79	1.43	1.68	1.52	0.37	-1.67	-1.7	1, 25
NGC 7582	35	0.31	2.24	2.23	2.25	1.29	-0.33	-0.4	4, 34
UGC 4013	32	...	0.55	0.82	0.55	0.61	-1.86	-1.99	AC345,
He 2-10	9.1	0.93	3.34	2.98	3.34	1.92	0.58	0.43	AH173, 37
IC 342	529	0.32	1.59	1.79	1.61	0.32	-2	-1.81	1, 17
IC 676	6.2	...	2.9	2.69	2.9	1.59	0.12	-0.04	11,
Maffei 2	23.3	0.54	3.96	3.41	3.96	2.41	0.42	0.24	AH407, 32
(U)LIRGs									
Arp 055	2.2+0.8	...	4	3.43	4	2.89	1.15	1.08	5,
Arp 148	0.24	...	5.66	4.56	5.66	5.02	3.16	2.88	7,
Arp 193	2.9	...	3.84	3.32	3.84	2.94	1.37	1.34	5,
Arp 220	0.34+0.22	...	6.02	4.81	6.02	5.43	3.81	3.55	7,
IC 0883	2.2	...	4.14	3.53	4.14	...	1.61	1.58	AB370,
IC 1623	15	...	3	2.75	3	2.13	0.14	0.22	AS267,
IC 5179	33	...	2.1	2.14	2.1	1.58	-0.56	-0.57	4,
III Zw 35	0.18	...	5.77	4.64	5.77	5.27	3.63	3.35	7,
IR 00335-2732	0.36	...	4.8	3.98	4.8	5.12	2.57	2.19	AN054,
IR 00506+7248	3.2	...	3.41	3.03	3.41	2.28	1.05	0.93	11,
IR 01364-1042	0.19	...	5.59	4.52	5.59	5.33	3.29	2.93	7,
IR 03056+2034	0.47	...	5.12	4.19	5.12	3.98	2.45	2.14	11,
IR 05189-2524	0.22	...	5.76	4.63	5.76	5.09	3.57	3.03	7,
IR 05414+5840	4.9	...	3.72	3.24	3.72	2.84	0.92	0.88	AS192+AM293,
IR 07329+1149	5.1	...	3.4	3.02	3.4	2.45	1.06	0.91	AC685+AC345,
IR 08071+0509	1.2	...	4.18	3.55	4.18	3.47	1.63	1.54	AB660,
IR 10039-3338	0.72	...	4.58	3.83	4.58	4.29	2.33	1.91	11,
IR 10173+0828	0.13	...	5.98	4.78	5.98	5.15	3.58	3.06	AS530,
IR 10565+2448	0.80	...	4.57	3.82	4.57	4.18	2.33	2.21	7,
IR 11506-3851	3.8	...	3.68	3.21	3.68	3.51	1.44	1.08	AM93,
IR 12112+0305	0.16+0.12	...	5.56	4.49	5.56	5	3.33	3.04	AN122,
IR 13126+2452	0.36	...	5.74	4.62	5.74	4.38	3.18	2.62	11,
IR 16399-0937	10.8+5.1	...	2.4	2.35	2.4	1.33	-0.09	-0.16	AB660,
IR 17138-1017	5.9	...	3.16	2.86	3.16	1.97	0.75	0.55	4,
IR 17208-0014	0.58	...	5.14	4.21	5.14	4.63	2.97	2.71	AH640,

TABLE 2 — Continued

Name	Diameter	$\log \Sigma_{\text{HI}}$	$\log^a \Sigma_{\text{H}_2}$	$\log^b \Sigma_{\text{H}_2}$	$\log^a \Sigma_{\text{gas}}$	$\log \Sigma_{\text{den}}$	$\log \Sigma_{\text{IR}}$	$\log \Sigma_{\text{RC}}$	Ref.
	[arcsec]			$[\text{M}_{\odot} \text{pc}^{-2}]$			$[\text{M}_{\odot} \text{yr}^{-1} \text{kpc}^{-2}]$		
IR 17526+3253	1.6+1.3	...	3.87	3.35	3.87	2.98	1.08	0.97	AM293,
IR 18090+0130	3.0	...	3.59	3.15	3.59	2.5	1.09	1.06	AB275,
IR 18293-3413	12	...	3.1	2.82	3.1	2.16	0.49	0.45	4,
IR 20550+1656	7.3+5.1	...	2.49	2.41	2.49	1.6	0.27	-0.01	AT149,
IR 22025+4205	1.0	...	4.44	3.73	4.44	4.18	1.95	1.79	AM293,
IR 23365+3604	0.21	...	5.55	4.49	5.55	5.18	3.28	3.07	AB660,
Mrk 0231	0.44	...	5.12	4.2	5.12	4.99	3.35	3.35	5,
Mrk 0266	13	...	2.58	2.47	2.58	1.14	0.07	0.07	5,
Mrk 0273	0.32+0.17	...	5.4	4.38	5.4	5.07	3.25	3.29	7,
Mrk 0331	2.53	...	4.2	3.57	4.2	3.35	1.55	1.3	AC243,
Mrk 1027	11	...	2.53	2.44	2.53	1.61	-0.22	-0.1	5,
NGC 0023	8.0	...	2.91	2.69	2.91	1.85	0.35	0.26	AD255,
NGC 0034	0.4	...	5.62	4.54	5.62	5.37	3.09	2.82	7,
NGC 0695	13	...	2.59	2.47	2.59	1.65	-0.18	-0.1	5,
NGC 0828	12	...	3.11	2.83	3.11	1.46	0.09	0.11	4,
NGC 1068	7.3	...	4.46	3.75	4.46	3.8	1.92	2.21	BG066,
NGC 1144	10	...	2.82	2.63	2.82	1.59	-0.08	0.44	AC205,
NGC 1365	20	...	3.45	3.06	3.45	2.7	0.55	0.23	AC348,
NGC 1614	2.2	...	4.3	3.64	4.3	3.22	1.96	1.71	AL503,
NGC 2146	27	...	3.02	2.76	3.02	2.21	0.44	0.42	3,
NGC 2369	28	...	2.33	2.3	2.33	1.53	-0.43	-0.48	10,
NGC 2388	5.5	...	3.41	3.03	3.41	2.45	0.87	0.58	11,
NGC 2623	0.46	...	5.39	4.38	5.39	4.49	3.07	2.91	7,
NGC 3034	43	...	3.46	3.07	3.46	2.44	1.05	0.87	AW624+AS250,
NGC 3110	20	...	2.16	2.18	2.16	1.11	-0.38	-0.24	5,
NGC 3256	12	...	3.49	3.09	3.49	2.56	0.95	0.91	AS412+AR531,
NGC 3690	27	...	2.41	2.35	2.41	1.63	0.3	0.21	AY102,
NGC 5135	6.5+0.7	...	3.48	3.08	3.48	2.75	0.76	0.91	8,
NGC 5653	19	...	2.27	2.25	2.27	1.19	-0.32	-0.44	5,
NGC 6240	8.6	...	3.09	2.81	3.09	2.67	0.57	0.98	4,
NGC 6701	22	...	2.38	2.33	2.38	1.32	-0.49	-0.48	4,
NGC 6921	4.1	...	3.8	3.3	3.8	3.04	0.97	0.46	AC264,
NGC 7130	0.6	...	5.51	4.46	5.51	4.71	2.79	2.96	AK394,
NGC 7469	3.3	...	3.91	3.37	3.91	3.03	1.56	1.47	AL490,
NGC 7552	7.2+6.1	...	3.5	3.09	3.5	2.64	1.09	0.74	AS721,
NGC 7591	0.94	...	4.71	3.91	4.71	3.59	2.07	1.92	AC685,
NGC 7771	16.97	...	2.59	2.48	2.59	2.05	0.01	-0.06	5,
UGC 1845	3.1	...	3.8	3.29	3.8	2.88	1.15	1.07	AC301+AT149,
UGC 5101	0.41	...	5.12	4.2	5.12	4.84	2.93	3.26	AA095+AS402,
VII Zw 31	3.6	...	3.65	3.19	3.65	2.66	0.76	0.76	4,
ZW 049.057	0.54	...	5.1	4.18	5.1	4.7	2.92	2.5	5,

REFERENCES. — **Radio map:** [1] Condon (1987); [2] Buczylowski & Beck (1987); [3] Braun et al. (2007); [4] Condon et al. (1996); [5] Condon et al. (1990); [6] Irwin et al. (1999); [7] Condon et al. (1991); [8] Ulvestad & Wilson (1989); [9] Condon et al. (2002); [10] Mauch et al. (2008); [11] NRAO Image Archive; [12] Becker et al. (2003).  $\Sigma_{\text{HI}}$ : [13] Walter et al. (2008); [14] Chung et al. (2009a); [15] van der Hulst (2002); [16] Hunter et al. (2012); [17] Martin (1998); [18] Cayatte et al. (1994); [19] Rhee & van Albada (1996); [20] Chamaraux et al. (1986); [21] Giovanardi et al. (1983); [22] Fouque (1984); [23] Bottinelli et al. (1970); [24] Whiteoak & Gardner (1977); [25] Laine & Gottesman (1998); [26] Ott et al. (2001); [27] Stanford (1990); [28] Ondrechen et al. (1989); [29] Saikia et al. (1990); [30] Irwin & Seaquist (1991); [31] Noordermeer et al. (2005); [32] Hurt et al. (1996); [33] Ryan-Weber et al. (2003); [34] Freeland et al. (2009); [35] Helou et al. (1981); [36] Liszt & Dickey (1995); [37] Kobulnicky et al. (1995); [38] Oosterloo et al. (2010); [39] Gallagher et al. (1975); [40] Li & Seaquist (1994).

NOTE. — a - the molecular gas mass (or total gas mass) is calculated using a fixed CO-to-H<sub>2</sub> conversion factor value of  $4.6 \text{ M}_{\odot} (\text{K km s}^{-1} \text{pc}^2)^{-1}$ ; b - the molecular gas mass is calculated using continuously-varying  $\alpha_{\text{CO}}$ . The (J)VLA observation project codes were given for the radio images reduced in this work. Two project codes were given in the cases that the data sets from two different (J)VLA configurations were combined. For interacting galaxies which clearly show two independent components, such as Arp 055 and Arp 220, we gave the radio sizes for both components.

## APPENDIX

## A. CALCULATING GAS MASS AND SFR

## A.1 Atomic Gas Mass

As H I emission is optically thin for most galaxies and does not suffer from extinction by interstellar dust, emission of H I can be converted directly into H I mass. The H I masses have been calculated from the H I fluxes using:

$$M(\text{H I}) [M_{\odot}] = 2.36 \times 10^5 \times D_L^2 \times F(\text{H I}) \quad (\text{A1})$$

where  $D_L$  is the distance to the source in Mpc and  $F(\text{H I})$  is the H I flux in units of  $\text{Jy km s}^{-1}$ . Given the fact that most of our objects are seen at low inclinations, we did not attempt to correct for any unknown optical depth effects. We assume that H I emissions in all galaxies are optically thin. If there were significant self-absorption, this would cause the derived H I masses to be underestimated.

## A.2 Molecular Gas Mass

The CO line luminosity  $L'_{\text{CO}}$  was calculated from the formula:

$$L'_{\text{CO}} = 3.25 \times 10^7 \times S_{\text{CO}} \Delta v \times \nu_{\text{obs}}^{-2} \times D_L^2 \quad (\text{A2})$$

where  $L'_{\text{CO}}$  is in  $\text{K km s}^{-1} \text{ pc}^2$ ,  $S_{\text{CO}} \Delta v$  in  $\text{Jy km s}^{-1}$ , distance  $D_L$  in Mpc and observation frequency  $\nu_{\text{obs}}$  of CO (1-0) for nearby galaxies is 115.27 GHz. The molecular gas mass can be derived from  $L'_{\text{CO}}$  with an empirical derivation of the CO-H<sub>2</sub> conversion factor ( $\alpha_{\text{CO}}$ ) which assumes a linear conversion relation:  $M(\text{H}_2 + \text{He}) (M_{\odot}) = \alpha_{\text{CO}} \times L'_{\text{CO}} (\text{K km s}^{-1})$ . The Galactic conversion factor value is  $\alpha_{\text{CO}} = 4.6 M_{\odot} (\text{K km s}^{-1} \text{ pc}^2)^{-1}$  (Young & Scoville 1991). A correction factor of 1.36 was applied to include helium.

## A.3 Dense Molecular Gas Mass

The line luminosity of dense molecular gas  $L'_{\text{HCN}}$  is then determined with the formula (GS04b):

$$L'_{\text{HCN}} (\text{K km s}^{-1} \text{ pc}^2)^{-1} = 3.25 \times 10^7 \times S_{\text{HCN}} \Delta v \times \nu_{\text{obs}}^{-2} \times D_L^2, \quad (\text{A3})$$

where  $S_{\text{HCN}} \Delta v$  in  $\text{Jy km s}^{-1}$ , distance  $D_L$  in Mpc and observation frequency  $\nu_{\text{obs}}$  of HCN (1-0) for local galaxies is 88.6 GHz. The dense molecular gas mass  $M_{\text{dense}}$  is obtained from  $L'_{\text{HCN}}$  using the formula given by GS04a:

$$M_{\text{dense}} (M_{\odot}) = 10 \times L'_{\text{HCN}} (\text{K km s}^{-1} \text{ pc}^2)^{-1} \quad (\text{A4})$$

which assumed a conversion factor of  $10 M_{\odot} (\text{K km s}^{-1} \text{ pc}^2)^{-1}$  between  $L'_{\text{HCN}}$  and dense molecular gas mass.

## A.4 The SFRs

The SFRs calibration of Bell (2003) which takes into account the effect of the reduced efficiency of IR and radio emission from low-luminosity galaxies, along with correcting for old stellar populations, is

$$\text{SFR}(\text{IR}) = \begin{cases} 1.57 \times 10^{-10} L_{\text{IR}} (1 + \sqrt{10^9/L_{\text{IR}}}), & L_{\text{IR}} > 10^{11}, \\ 1.17 \times 10^{-10} L_{\text{IR}} (1 + \sqrt{10^9/L_{\text{IR}}}), & L_{\text{IR}} \leq 10^{11}, \end{cases} \quad (\text{A5})$$

$$\text{SFR}(\text{RC}) = \begin{cases} 5.52 \times 10^{-22} L_{1.4\text{GHz}}, & L > L_c, \\ (5.52 \times 10^{-22} L_{1.4\text{GHz}}) / [0.1 + 0.9(L_{1.4\text{GHz}}/L_c)^{0.3}], & L \leq L_c. \end{cases} \quad (\text{A6})$$

Here, we define  $\text{SFR}(\text{IR})$  and  $\text{SFR}(\text{RC})$  as the SFRs derived from total infrared luminosity and 1.4 GHz radio continuum luminosity, respectively. The SFRs is in units of  $M_{\odot} \text{ yr}^{-1}$ ,  $L_{\text{IR}}$  is given in units of  $L_{\odot}$ ,  $L_{1.4\text{GHz}}$  is in  $\text{W Hz}^{-1}$  and  $L_c = 6.4 \times 10^{21} \text{ W Hz}^{-1}$ , which is the 1.4 GHz radio luminosity of a  $\sim L_*$  galaxy.

Fig. 6 shows the comparison of the IR-based  $\text{SFR}(\text{IR})$  and RC-based  $\text{SFR}(\text{RC})$ . Overall, the two SFRs gave qualitatively identical results with scatter of only  $\sim 0.21$  dex. It is worth a quick note that the two SFRs of some individual galaxies can deviate substantially from each other, such as NGC 4394 and IRAS 12243-0036. This was also noted by Bell (2003), i.e., the above calibrations are more based on a galaxy-by-galaxy basis and some individual galaxies can deviate substantially from the mean behavior. The SFRs in our sample spanned a wide range, from  $\leq 1 M_{\odot} \text{ yr}^{-1}$  in some quiescent early type galaxies to more than  $\sim 480 M_{\odot} \text{ yr}^{-1}$  in strong starbursts.

As an excellent agreement was found between the two SFR estimators, using one over the other, therefore, did not alter our results of SF laws in any significant way. Here we show some examples of SF laws derived by adopting RC-based SFRs. Fig. 7 presents the relations between the densities of  $\text{SFR}(\text{RC})$  and molecular gas, total gas as well as dense gas. The derived slopes are  $N = 1.10 \pm 0.02$ ,  $N = 1.19 \pm 0.02$  and  $N = 0.98 \pm 0.02$ , respectively, agreeing very well with the same relations derived from IR-based SFRs.

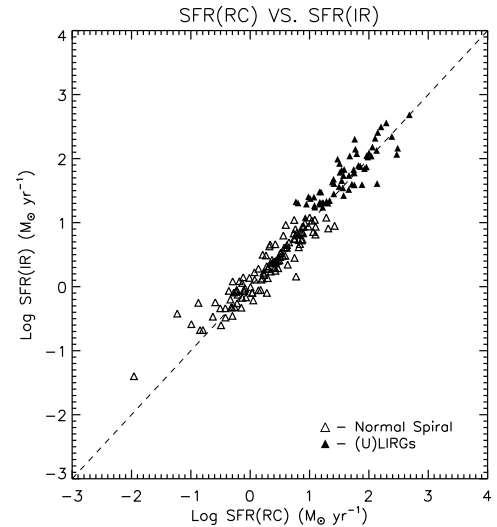


FIG. 6.— The distributions of  $\text{SFR}(\text{IR})$  and  $\text{SFR}(\text{RC})$  generally follow a trend denoted by the dashed line which is linear, suggesting that the two SFRs gave qualitatively identical results.

## B. RADIO SIZE MEASUREMENT

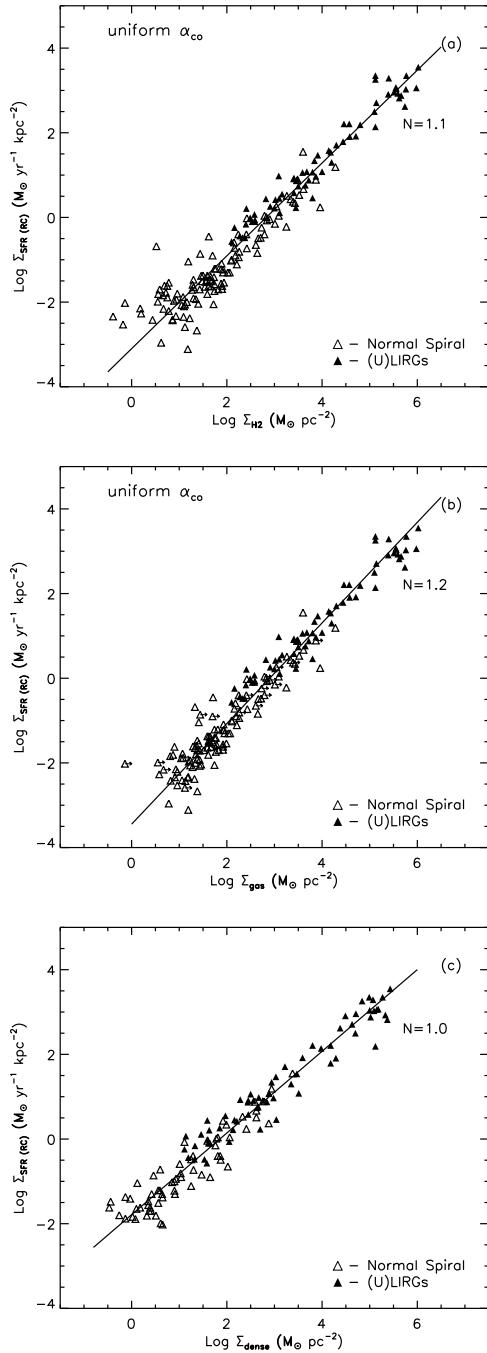


FIG. 7.— The SF laws derived by using RC-based SFRs: (a) SFR(RC) vs.  $H_2$ ; (b) SFR(RC) vs. total gas; (c) SFR(RC) vs. dense gas. The molecular gas (and total gas) here is deduced by adopting constant Galactic  $\alpha_{CO}$ . The SF laws derived by adopting RC-based SFRs agree well with the results using IR-based SFRs.

Most of our radio images are based on 1.4 GHz (L-band) RC observations. However, for the compact starbursts whose radio emissions are unresolved by the highest resolution ( $\sim 1''.5$ ) of 1.4 GHz VLA maps, the higher frequency (J)VLA observations were adopted to achieve higher resolutions. It is worth noting that the high-resolution maps may miss extended low-brightness components, and thus the extended global structure of the source. We made every effort to ensure that each galaxy can be resolved yet little missing flux due to high interferometer resolution.

The galaxy major/minor axis was determined by fitting 2D Gaussian to each radio map using the *AZPS* task IMFIT. In general, we tend to choose the resolved radio maps with the lowest resolution for each galaxy. Around 98% (178/181) of our galaxies were resolved, among which  $\sim 88\%$  (158/181) were fully resolved with deconvolved sizes larger than beam sizes, and  $\sim 11\%$  (20/181) galaxies were partially resolved (i.e., those with deconvolved sizes larger than 1/2 beam size). As for the cases where one-component Gaussian model failed, such as the galaxies with complex morphologies, we measured their effective diameters, which contains half of the integrated radio flux, instead.

The radio sizes of our galaxies range between  $0''.2$  to  $13'$ , corresponding to  $\sim 0.2$  kpc to 20 kpc in linear scale. The typical values for normal spirals were 1 – 10 kpc, while the size of (U)LIRGs were significantly smaller with typical values being a few kpc or less. Especially for those extremely compact starbursts, their high surface brightness radio emission is restricted at nuclear region within an extent of a few hundreds pc scale.

One important caveat on the use of radio size, however, is the possibility of an active galactic nucleus (AGN) contributing to the radio emission. Luckily, the interferometers with very long baselines (e.g., VLBA and VLBI) have extremely high resolution to easily pick out AGN. Our trick is to assume AGN are point sources and estimate their radio contribution through highest angular resolution observations to galaxy radio cores by VLBA/VLBI. We found that radio cores contributed only a small fraction ( $\leq 10\%$ ) of the total radio flux for most of our Seyfert galaxies. As for those Seyfert galaxies whose radio core contribute more than 10% of the total RC flux, we subtracted point source equivalent to that value in lower resolution VLA map and then fitted a Gaussian to the difference. Thus, we took the average of the upper and lower values as a approximate estimate of the radio size in these Seyfert galaxies.

 C. CORRELATION WITH FIR COLOR  $C(60/100)$ 

Fig. 8 presents  $\Sigma_{SFR}/\Sigma_{dense}$  versus  $C(60/100)$  for HCN sample. The  $\Sigma_{SFR}/\Sigma_{dense}$  shows a weak dependence on the  $C(60/100)$ , or dust temperature  $T_{dust}$  since  $C(60/100)$  is a good estimator of  $T_{dust}$  (Chanial et al. 2007; Díaz-Santos et al. 2010). The  $\Sigma_{SFR}/\Sigma_{dense}$  ratio gets slightly higher for warmer dust temperature.

We found a rather strong FIR color dependence of  $\Sigma_{SFR}$ . Fig. 9 plots our IR-based SFR versus  $C(60/100)$  for the 175 galaxies with  $C(60/100) > 0.25$ . Fitting all the points in the figure derives a relation:  $\log \Sigma_{SFR} = (10.09 \pm 0.46) \log C(60/100) + (2.68 \pm 0.17)$ . And this fitted relationship was used in Lu et al. (ApJL, submitted) in roughly estimating SFR surface density from FIR color.

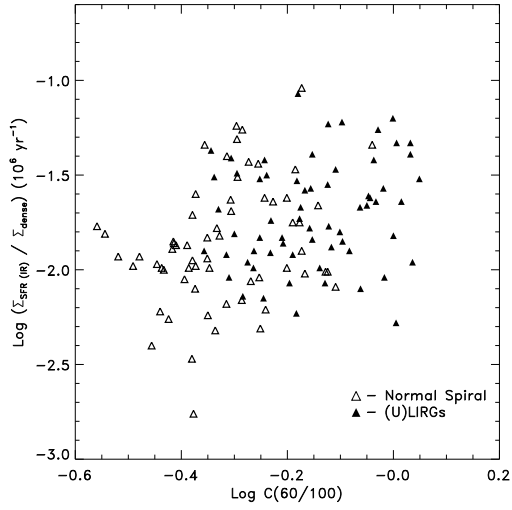


FIG. 8.—  $\Sigma_{\text{SFR}}/\Sigma_{\text{dense}}$  ratio as a function of the FIR color  $[C(60/100)]$ .

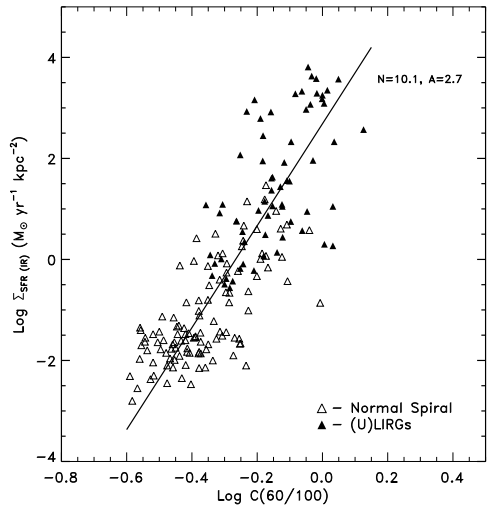


FIG. 9.—  $\Sigma_{\text{SFR}}$  as a function of the FIR color  $[C(60/100)]$ .

## REFERENCES

- Baan, W. A., Henkel, C., Loenen, A. F., Baudry, A., & Wiklind, T. 2008, *A&A*, 477, 747
- Baan, W. A., & Klöckner, H.-R. 2006, *A&A*, 449, 559
- Bayet, E., Gerin, M., Phillips, T. G., & Contursi, A. 2009, *MNRAS*, 399, 264
- Becker, R. H., Helfand, D. J., White, R. L., Gregg, M. D., & Laurent-Muehleisen, S. A. 2003, *VizieR Online Data Catalog*, 8071, 0
- Bell, E. F. 2003, *ApJ*, 586, 794
- Bigiel, F., Leroy, A., Walter, F., Brinks, E., de Blok, W. J. G., Madore, B., & Thornley, M. D. 2008, *AJ*, 136, 2846
- Bigiel, F. et al. 2011, *ApJL*, 730, L13
- Blanc, G. A., Heiderman, A., Gebhardt, K., Evans, II, N. J., & Adams, J. 2009, *ApJ*, 704, 842
- Bolatto, A. D. et al. 2011, *ApJ*, 741, 12
- Bolatto, A. D., Wolfire, M., & Leroy, A. K. 2013, *ARA&A*, 51, 207
- Boquien, M., Lisenfeld, U., Duc, P.-A., Braine, J., Bournaud, F., Brinks, E., & Charmandaris, V. 2011, *A&A*, 533, A19
- Boselli, A., Lequeux, J., & Gavazzi, G. 2002, *Ap&SS*, 281, 127
- Bothwell, M. S. et al. 2010, *MNRAS*, 405, 219
- Bottinelli, L., Chamaraux, P., Gouguenheim, L., & Lauqué, R. 1970, *A&A*, 6, 453
- Bouché, N. et al. 2007, *ApJ*, 671, 303
- Bourne, N., Dunne, L., Ivison, R. J., Maddox, S. J., Dickinson, M., & Frayer, D. T. 2011, *MNRAS*, 410, 1155
- Braun, R., Oosterloo, T. A., Morganti, R., Klein, U., & Beck, R. 2007, *A&A*, 461, 455
- Bryant, P. M., & Scoville, N. Z. 1999, *AJ*, 117, 2632
- Buczkowski, U. R., & Beck, R. 1987, *A&AS*, 68, 171
- Calzetti, D., Liu, G., & Koda, J. 2012, *ApJ*, 752, 98
- Carilli, C. L., & Taylor, G. B. 2000, *ApJ*, 532, L95
- Carilli, C. L., Wrobel, J. M., & Ulvestad, J. S. 1998, *AJ*, 115, 928
- Cayatte, V., Kotanyi, C., Balkowski, C., & van Gorkom, J. H. 1994, *AJ*, 107, 1003
- Chamaraux, P., Balkowski, C., & Fontanelli, P. 1986, *A&A*, 165, 15
- Chanical, P., Flores, H., Guiderdoni, B., Elbaz, D., Hammer, F., & Vigroux, L. 2007, *A&A*, 462, 81
- Chen, J., Lo, K. Y., Gruendl, R. A., Peng, M.-L., & Gao, Y. 2002, *AJ*, 123, 720
- Chung, A., van Gorkom, J. H., Kenney, J. D. P., Crawl, H., & Vollmer, B. 2009a, *AJ*, 138, 1741
- Chung, E. J., Rhee, M.-H., Kim, H., Yun, M. S., Heyer, M., & Young, J. S. 2009b, *ApJS*, 184, 199
- Cole, G. H. J., Pedlar, A., Holloway, A. J., & Mundell, C. G. 1999, *MNRAS*, 310, 1033
- Condon, J. J. 1987, *ApJS*, 65, 485
- , 1992, *ARA&A*, 30, 575
- Condon, J. J., Anderson, M. L., & Helou, G. 1991, *ApJ*, 376, 95
- Condon, J. J., Cotton, W. D., Greisen, E. W., Yin, Q. F., Perley, R. A., Taylor, G. B., & Broderick, J. J. 1998, *AJ*, 115, 1693
- , *VizieR Online Data Catalog*, 8065, 0
- Condon, J. J., Helou, G., Sanders, D. B., & Soifer, B. T. 1990, *ApJS*, 73, 359
- , 1996, *ApJS*, 103, 81
- Crocker, A. et al. 2012, *MNRAS*, 421, 1298
- Crocker, A. F., Bureau, M., Young, L. M., & Combes, F. 2011, *MNRAS*, 410, 1197
- Crosthwaite, L. P., Turner, J. L., Buchholz, L., Ho, P. T. P., & Martin, R. N. 2002, *AJ*, 123, 1892
- Curran, S. J., Aalto, S., & Booth, R. S. 2000, *A&AS*, 141, 193
- Daddi, E. et al. 2010, *ApJ*, 714, L118
- Díaz-Santos, T. et al. 2010, *ApJ*, 723, 993
- Downes, D., & Solomon, P. M. 1998, *ApJ*, 507, 615
- Elfhag, T., Booth, R. S., Hoeglund, B., Johansson, L. E. B., & Sandqvist, A. 1996, *A&AS*, 115, 439
- Evans, II, N. J. 1999, *ARA&A*, 37, 311
- Evans, II, N. J. 2008, in *Astronomical Society of the Pacific Conference Series*, Vol. 390, *Pathways Through an Eclectic Universe*, ed. J. H. Knapen, T. J. Mahoney, & A. Vazdekis, 52
- Feldmann, R. 2013, *MNRAS*, 433, 1910
- Fouque, P. 1984, *A&AS*, 55, 55
- Freeland, E., Stilp, A., & Wilcots, E. 2009, *AJ*, 138, 295
- Fumagalli, M., Krumholz, M. R., Prochaska, J. X., Gavazzi, G., & Boselli, A. 2009, *ApJ*, 697, 1811
- Gallagher, J. S., Faber, S. M., & Balick, B. 1975, *ApJ*, 202, 7
- Gao, Y., & Solomon, P. M. 1999, *ApJ*, 512, L99
- , 2004a, *ApJS*, 152, 63
- , 2004b, *ApJ*, 606, 271
- García-Burillo, S., Usero, A., Alonso-Herrero, A., Graciá-Carpio, J., Pereira-Santaella, M., Colina, L., Planesas, P., & Arribas, S. 2012, *A&A*, 539, A8
- García-Ruiz, I., Sancisi, R., & Kuijken, K. 2002, *A&A*, 394, 769
- Gardan, E., Braine, J., Schuster, K. F., Brouillet, N., & Sievers, A. 2007, *A&A*, 473, 91
- Genzel, R. et al. 2010, *MNRAS*, 407, 2091
- Giovanardi, C., Krumm, N., & Salpeter, E. E. 1983, *AJ*, 88, 1719
- Graciá-Carpio, J., García-Burillo, S., & Planesas, P. 2008, *APSS*, 313, 331
- Gratier, P. et al. 2010, *A&A*, 522, A3
- Helfer, T. T., Thornley, M. D., Regan, M. W., Wong, T., Sheth, K., Vogel, S. N., Blitz, L., & Bock, D. C.-J. 2003, *ApJS*, 145, 259
- Helou, G., Salpeter, E. E., Giovanardi, C., & Krumm, N. 1981, *ApJS*, 46, 267
- Helou, G., Soifer, B. T., & Rowan-Robinson, M. 1985, *ApJ*, 298, L7
- Hibbard, J. E., van der Hulst, J. M., Barnes, J. E., & Rich, R. M. 2001a, *AJ*, 122, 2969
- Hibbard, J. E., van Gorkom, J. H., Rupen, M. P., & Schiminovich, D. 2001b, in *Astronomical Society of the Pacific Conference Series*, Vol. 240, *Gas and Galaxy Evolution*, ed. J. E. Hibbard, M. Rupen, & J. H. van Gorkom, 657
- Hodge, J. A., Carilli, C. L., Walter, F., de Blok, W. J. G., Riechers, D., Daddi, E., & Lentati, L. 2012, *ApJ*, 760, 11
- Huettmeister, S., Henkel, C., Mauersberger, R., Brouillet, N., Wiklind, T., & Millar, T. J. 1995, *A&A*, 295, 571
- Hunter, D. A. et al. 2012, *AJ*, 144, 134
- Hurt, R. L., Turner, J. L., & Ho, P. T. P. 1996, *ApJ*, 466, 135
- Imanishi, M., Nakanishi, K., Tamura, Y., Oi, N., & Kohno, K. 2007, *AJ*, 134, 2366
- Imanishi, M., Nakanishi, K., Tamura, Y., & Peng, C.-H. 2009, *AJ*, 137, 3581
- Iono, D. et al. 2009, *ApJ*, 695, 1537
- Irwin, J. A., English, J., & Sorathia, B. 1999, *AJ*, 117, 2102
- Irwin, J. A., & Seaquist, E. R. 1991, *ApJ*, 371, 111
- Ivison, R. J., Papadopoulos, P. P., Smail, I., Greve, T. R., Thomson, A. P., Xilouris, E. M., & Chapman, S. C. 2011, *MNRAS*, 412, 1913
- Joint Iras Science, W. G. 1994, *VizieR Online Data Catalog*, 2125, 0
- Juneau, S., Narayanan, D. T., Moustakas, J., Shirley, Y. L., Bussmann, R. S., Kennicutt, Jr., R. C., & Vanden Bout, P. A. 2009, *ApJ*, 707, 1217
- Kelly, B. C. 2007, *ApJ*, 665, 1489
- Kennicutt, Jr., R. C. 1998, *ApJ*, 498, 541
- Kennicutt, Jr., R. C. 2008, in *Astronomical Society of the Pacific Conference Series*, Vol. 390, *Pathways Through an Eclectic Universe*, ed. J. H. Knapen, T. J. Mahoney, & A. Vazdekis, 149
- Kennicutt, Jr., R. C. et al. 2007, *ApJ*, 671, 333
- Kobulnicky, H. A., Dickey, J. M., Sargent, A. I., Hogg, D. E., & Conti, P. S. 1995, *AJ*, 110, 116
- Komatsu, E. et al. 2011, *ApJS*, 192, 18
- Krips, M., Crocker, A. F., Bureau, M., Combes, F., & Young, L. M. 2010, *MNRAS*, 407, 2261
- Krips, M., Neri, R., García-Burillo, S., Martín, S., Combes, F., Graciá-Carpio, J., & Eckart, A. 2008, *ApJ*, 677, 262
- Krumholz, M. R., Dekel, A., & McKee, C. F. 2012, *ApJ*, 745, 69
- Krumholz, M. R., Leroy, A. K., & McKee, C. F. 2011, *ApJ*, 731, 25
- Krumholz, M. R., McKee, C. F., & Tumlinson, J. 2008, *ApJ*, 689, 865
- , 2009, *ApJ*, 693, 216
- Kuno, N. et al. 2007, *PASJ*, 59, 117
- Laine, S., & Gottesman, S. T. 1998, *MNRAS*, 297, 1041
- Leroy, A., Bolatto, A. D., Simon, J. D., & Blitz, L. 2005, *ApJ*, 625, 763
- Leroy, A. K. et al. 2011, *ApJ*, 737, 12

- . 2009, *AJ*, 137, 4670
- Leroy, A. K., Walter, F., Brinks, E., Bigiel, F., de Blok, W. J. G., Madore, B., & Thornley, M. D. 2008, *AJ*, 136, 2782
- Leroy, A. K. et al. 2013, *AJ*, 146, 19
- Li, J. G., & Seaquist, E. R. 1994, *AJ*, 107, 1953
- Lisenfeld, U. et al. 2007, *A&A*, 462, 507
- Liszt, H. S., & Dickey, J. M. 1995, *AJ*, 110, 998
- Liu, F., & Gao, Y. 2010, *ApJ*, 713, 524
- Liu, L., & Gao, Y. 2012, *Science China Physics, Mechanics, and Astronomy*, 55, 347
- Lucero, D. M., & Young, L. M. 2007, *AJ*, 134, 2148
- Maiolino, R., Ruiz, M., Rieke, G. H., & Papadopoulos, P. 1997, *ApJ*, 485, 552
- Mao, M. Y., Huynh, M. T., Norris, R. P., Dickinson, M., Frayer, D., Helou, G., & Monkiewicz, J. A. 2011, *ApJ*, 731, 79
- Martin, C. L., & Kennicutt, Jr., R. C. 2001, *ApJ*, 555, 301
- Martin, M. C. 1998, *A&AS*, 131, 73
- Matsushita, S., Kawabe, R., Kohno, K., Tosaki, T., & Vila-Vilaró, B. 2010, *PASJ*, 62, 409
- Mauch, T., Murphy, T., Buttery, H. J., Curran, J., Hunstead, R. W., Piestrzynski, B., Ropertson, J. G., & Sadler, E. M. 2008, *VizieR Online Data Catalog*, 8081, 0
- Mirabel, I. F., & Sanders, D. B. 1989, *ApJ*, 340, L53
- Momjian, E., Romney, J. D., Carilli, C. L., Troland, T. H., & Taylor, G. B. 2003, *ApJ*, 587, 160
- Moshir, M. et al. 1993, *VizieR Online Data Catalog*, 2156, 0
- Moshir, M. et al. 1990, in *Bulletin of the American Astronomical Society*, Vol. 22, *Bulletin of the American Astronomical Society*, 1325
- Murgia, M., Crapsi, A., Moscadelli, L., & Gregorini, L. 2002, *A&A*, 385, 412
- Murgia, M., Helfer, T. T., Ekers, R., Blitz, L., Moscadelli, L., Wong, T., & Paladino, R. 2005, *A&A*, 437, 389
- Murphy, E. J., Armus, L., Helou, G., Braun, R., & SINGS Team. 2006a, in *Astronomical Society of the Pacific Conference Series*, Vol. 357, *Astronomical Society of the Pacific Conference Series*, ed. L. Armus & W. T. Reach, 194
- Murphy, E. J. et al. 2006b, *ApJ*, 651, L111
- Murphy, E. J., Helou, G., Kenney, J. D. P., Armus, L., & Braun, R. 2008, *ApJ*, 678, 828
- Narayanan, D., Krumholz, M., Ostriker, E. C., & Hernquist, L. 2011, *MNRAS*, 418, 664
- Narayanan, D., Krumholz, M. R., Ostriker, E. C., & Hernquist, L. 2012, *MNRAS*, 421, 3127
- Nguyen, Q.-R., Jackson, J. M., Henkel, C., Truong, B., & Mauersberger, R. 1992, *ApJ*, 399, 521
- Nishiyama, K., & Nakai, N. 2001, *PASJ*, 53, 713
- Noordermeer, E., van der Hulst, J. M., Sancisi, R., Swaters, R. A., & van Albada, T. S. 2005, *A&A*, 442, 137
- Ondrechen, M. P., van der Hulst, J. M., & Hummel, E. 1989, *ApJ*, 342, 39
- Oosterloo, T. et al. 2010, *MNRAS*, 409, 500
- Ott, M., Whiteoak, J. B., Henkel, C., & Wielebinski, R. 2001, *A&A*, 372, 463
- Paglion, T. A. D. et al. 2001, *ApJS*, 135, 183
- Papadopoulos, P. P., van der Werf, P., Isaak, K., & Xilouris, E. M. 2010, *ApJ*, 715, 775
- Pihlström, Y. M., Conway, J. E., Booth, R. S., Diamond, P. J., & Polatidis, A. G. 2001, *A&A*, 377, 413
- Price, R., & Duric, N. 1992, *ApJ*, 401, 81
- Rahman, N. et al. 2011, *ApJ*, 730, 72
- . 2012, *ApJ*, 745, 183
- Regan, M. W., Thornley, M. D., Helfer, T. T., Sheth, K., Wong, T., Vogel, S. N., Blitz, L., & Bock, D. C.-J. 2001, *ApJ*, 561, 218
- Rhee, M.-H., & van Albada, T. S. 1996, *A&AS*, 115, 407
- Rice, W., Lonsdale, C. J., Soifer, B. T., Neugebauer, G., Kopan, E. L., Lloyd, L. A., de Jong, T., & Habing, H. J. 1988, *ApJS*, 68, 91
- Riechers, D. A. 2012, in *American Astronomical Society Meeting Abstracts*, Vol. 219, *American Astronomical Society Meeting Abstracts* 219, 340.14
- Rujopakarn, W., Rieke, G. H., Eisenstein, D. J., & Juneau, S. 2011, *ApJ*, 726, 93
- Ryan-Weber, E. V., Webster, R. L., & Staveley-Smith, L. 2003, *MNRAS*, 343, 1195
- Sadler, E. M. 2001, in *Astronomical Society of the Pacific Conference Series*, Vol. 240, *Gas and Galaxy Evolution*, ed. J. E. Hibbard, M. Rupen, & J. H. van Gorkom, 445
- Sadler, E. M., Oosterloo, T. A., Morganti, R., & Karakas, A. 2000, *AJ*, 119, 1180
- Sage, L. J. 1993, *A&AS*, 100, 537
- Saikia, D. J., Unger, S. W., Pedlar, A., Yates, G. J., Axon, D. J., Wolstencroft, R. D., Taylor, K., & Gyldenkerne, K. 1990, *MNRAS*, 245, 397
- Saintonge, A. et al. 2012, *ApJ*, 758, 73
- Sanders, D. B., Mazzarella, J. M., Kim, D.-C., Surace, J. A., & Soifer, B. T. 2003, *AJ*, 126, 1607
- Sanders, D. B., & Mirabel, I. F. 1996, *ARA&A*, 34, 749
- Sandstrom, K. M. et al. 2013, *ApJ*, 777, 5
- Sargent, M. T. et al. 2010, *ApJL*, 714, L190
- Schmidt, M. 1959, *ApJ*, 129, 243
- Schruba, A. et al. 2011, *AJ*, 142, 37
- Schruba, A., Leroy, A. K., Walter, F., & HERACLES Team. 2012, in *American Astronomical Society Meeting Abstracts*, Vol. 219, *American Astronomical Society Meeting Abstracts* 219, 346.02
- Schruba, A., Leroy, A. K., Walter, F., Sandstrom, K., & Rosolowsky, E. 2010, *ApJ*, 722, 1699
- Schuster, K. F., Kramer, C., Hitschfeld, M., Garcia-Burillo, S., & Mookerjee, B. 2007, *A&A*, 461, 143
- Smith, B. J., & Harvey, P. M. 1996, *ApJ*, 468, 139
- Sofue, Y., Koda, J., Nakanishi, H., Onodera, S., Kohno, K., Tomita, A., & Okumura, S. K. 2003, *PASJ*, 55, 17
- Solomon, P. M., Downes, D., & Radford, S. J. E. 1992, *ApJL*, 387, L55
- Stanford, S. A. 1990, *ApJ*, 358, 153
- Strickland, D. K., Heckman, T. M., Colbert, E. J. M., Hoopes, C. G., & Weaver, K. A. 2004, *ApJ*, 606, 829
- Swaters, R. A., & Balcells, M. 2002, *A&A*, 390, 863
- Swaters, R. A., van Albada, T. S., van der Hulst, J. M., & Sancisi, R. 2002, *A&A*, 390, 829
- Tacconi, L. J. et al. 2006, *ApJ*, 640, 228
- Taramopoulos, A., Payne, H., & Briggs, F. H. 2001, *A&A*, 365, 360
- Ulvestad, J. S., & Wilson, A. S. 1989, *ApJ*, 343, 659
- van der Hulst, J. M. 2002, in *Astronomical Society of the Pacific Conference Series*, Vol. 276, *Seeing Through the Dust: The Detection of HI and the Exploration of the ISM in Galaxies*, ed. A. R. Taylor, T. L. Landecker, & A. G. Willis, 84
- van Driel, W., Gao, Y., & Monnier-Ragaine, D. 2001, *A&A*, 368, 64
- Verley, S., Corbelli, E., Giovanardi, C., & Hunt, L. K. 2010, *A&A*, 510, A64
- Walter, F., Brinks, E., de Blok, W. J. G., Bigiel, F., Kennicutt, Jr., R. C., Thornley, M. D., & Leroy, A. 2008, *AJ*, 136, 2563
- Wang, B., & Heckman, T. M. 1996, *ApJ*, 457, 645
- Wang, M., Henkel, C., Chin, Y.-N., Whiteoak, J. B., Hunt, Cunningham, M., Mauersberger, R., & Muters, D. 2004, *A&A*, 422, 883
- Wang, W.-H., Lo, K. Y., Gao, Y., & Gruendl, R. A. 2001, *AJ*, 122, 140
- Whiteoak, J. B., & Gardner, F. F. 1977, *Australian Journal of Physics*, 30, 187
- Wong, T., & Blitz, L. 2002, *ApJ*, 569, 157
- Wu, J., Evans, II, N. J., Gao, Y., Solomon, P. M., Shirley, Y. L., & Vanden Bout, P. A. 2005, *ApJL*, 635, L173
- Wu, J., Evans, II, N. J., Shirley, Y. L., & Knez, C. 2010, *ApJS*, 188, 313
- Wyder, T. K. et al. 2009, *ApJ*, 696, 1834
- Young, J. S., & Knezek, P. M. 1989, *ApJ*, 347, L55
- Young, J. S., & Scoville, N. Z. 1991, *ARA&A*, 29, 581
- Young, J. S. et al. 1995, *ApJS*, 98, 219
- Young, L. M., Bendo, G. J., & Lucero, D. M. 2009, *AJ*, 137, 3053
- Young, L. M., Bureau, M., & Cappellari, M. 2008, *ApJ*, 676, 317
- Yun, M. S., Reddy, N. A., & Condon, J. J. 2001, *ApJ*, 554, 803
- Zhang, Z.-Y., Gao, Y., Henkel, C., Zhao, Y., Wang, J., Menten, K. M., & Güsten, R. 2014, *ApJ*, 784, L31